1

Tropical Atlantic biases
in the mean state, seasonal cycle, and interannual variations
for a coarse and a high resolution coupled climate model

5

6

7

8

9

Takeshi Doi[1,2], Gabriel A. Vecchi[2], Anthony J. Rosati[2], and Thomas L. Delworth[2]

11

12

1 Atmospheric and Oceanic Sciences Program, Princeton University, Princeton, NJ, U.S.A.
2 NOAA/Geophysical Fluid Dynamics Laboratory, Princeton, NJ, U.S.A.

15

16

17

20

21

22 ———————————————————————————————

Corresponding author address: Takeshi Doi, Geophysical Fluid Dynamics Laboratory/NOAA, Princeton University Forrestal Campus, 201 Forrestal Road, Princeton, NJ 08542, USA
Tel: +1-609-452-6511
Email: Takeshi.Doi@noaa.gov

Abstract:

Using two fully coupled ocean-atmosphere models (the Climate Model version 2.1 developed at the Geophysical Fluid Dynamics Laboratory, CM2.1 and CM2.5: a new high-resolution climate model based on CM2.1), the character and sources of SST and precipitation biases in the tropical Atlantic have been investigated. Although both models have warm SST biases in the eastern tropical Atlantic in the annual mean, CM2.5 successfully simulates reasonable rainfall over the northern South America. In the mean seasonal cycle, CM2.1 shows large seasonal meridional migration of the Intertropical Convergence Zone (ITCZ) compared to observations, which causes excessive Sahel rainfall and lack of northern South America rainfall in boreal summer. Those biases are also reduced in CM2.5.

CM2.5 shows much better simulation skills for the seasonal phase-locking of the interannual variations of the northern tropical Atlantic SST than CM2.1. In observation, the interannual SST anomaly in the northern tropical Atlantic develops in early winter, reaches its peak in boreal spring, and decays abruptly in boreal summer. In CM2.1, the decay of the interannual SST anomaly is slow and weak compared to observations. We found that it is due to an unrealistic air-sea coupled positive feedback linked with a subsurface doming of the thermocline in the northeastern tropical Atlantic, known as the Guinea Dome. In CM2.1, large meridional migrations of the ITCZ coupled with the warm SST anomaly in the

1   northern tropical Atlantic leads to the Ekman downwelling anomaly over the Guinea Dome

2   region. This suppresses the decay of the warm SST anomaly through entrainment in CM2.1.

3   Those biases are significantly reduced in CM2.5.

1

1. Introduction

3

4   Climate conditions over the tropical Atlantic Ocean can have far-reaching effects.

5 The sea surface temperature (SST) over the northern tropical Atlantic influences the

6 Atlantic hurricane activity (Emanuel 2005; Vecchi and Soden 2007). SST variation in the

7 northern tropical Atlantic also has potential impacts on rainfall over northern South

8 America and the Sahel region through the meridional migration of the Intertropical

9 Convergence Zone (ITCZ) and the West African Monsoon (Hagos and Cook 2008). Folland

10 et al. (2001) showed that the meridional gradient between the SST in the northern tropical

11 Atlantic and that in the Southern Hemisphere is more important than the remote influence

12 associated with ENSO for prediction of the northeastern South America rainfall. Hagos and

13 Cook (2009) discussed that the warm SST in the northeastern tropical Atlantic enhances the

14 westward moisture transport on to the Sahel region. Interestingly, the impacts of the

15 Atlantic variation are not restricted to the Atlantic Basin. Dommenget et al. (2006)

16 suggested the tropical Atlantic SST could modulate the ENSO period and its variance.

17 Zhang and Delworth (2006) showed that the Atlantic Ocean variations could influence the

18 India summer rainfall in multidecadal timescale. Also, Zhang et al. (2007) suggested that

19 the Atlantic multidecadal variability could play an important role on the evolution of the

20 Northern Hemisphere mean temperature. Sutton and Hodson (2005 and 2007) concluded

1   that the impacts of the North Atlantic SST could be an important driver of global climate

2   variation. Recently, Hodson et al. (2010) investigated global climate impacts of

3   multidecadal Atlantic SST variation by multimodel comparison. Kucharski et al. (2011)

4   suggested that the Atlantic warming in the 20th century might have reduced the

5   concomitant warming in the eastern tropical Pacific with a change of the Walker

6   circulation.

7   In the tropical Atlantic, three major climate modes on interannual timescale have

8   been identified: the Atlantic Niño/Niña (or Atlantic Zonal Mode), the Atlantic Meridional

9   Mode (or Atlantic Gradient Mode) and the Benguela Niño. Each of these three climate

10   modes is strongly phase-locked to the seasonal cycle. The Atlantic Niño is associated with a

11   warm SST anomaly in the eastern equatorial Atlantic, which is similar to the Pacific El

12   Niño and has its peak in boreal summer (Zebiak 1993; Carton and Huang 1994). The

13   Atlantic Meridional Mode (Servain 1991; Xie and Carton 2004 for a recent review) is

14   associated with the cross-equatorial meridional gradient of SST anomaly in the tropical

15   Atlantic in boreal spring. These climate modes have large impacts on rainfall over the

16   northeastern South America and the Sahel region (Kushnir et al. 2006). In addition, it is

17   recently suggested that the Atlantic Meridional Mode is significantly linked with the

18   Atlantic hurricane intensity and frequency (Kossin and Vimont 2007; Vimont and Kossin

19   2007). The Benguela Niño has its peak in boreal spring and is associated with the warm

20   SST anomaly around the Angola-Benguela Frontal Zone (Florenchie et al. 2003; Richter et

1   al. 2010), and has been connected to rainfall variations over Angola (Rouault et al. 2003).

2   These climate modes are tied to and influence oceanic conditions. In the tropical

3   Atlantic, two thermocline domes associated with ocean upwelling are found; the Angola

4   Dome in the southeastern tropical Atlantic and the Guinea Dome in the northeastern

5   tropical Atlantic (Mazeika 1967). Interannual variations of the Angola Dome in the South

6   Atlantic are strongly influenced by the Atlantic Niño (Doi et al. 2007), while the

7   interannual variations of the Guinea Dome are linked with the Atlantic Meridional Mode

8   (Doi et al. 2009; 2010). The subsurface ocean variations of the two upwelling domes have

9   potential impacts not only on the biological activity there (Binet et al. 2001; Signorini et al.

10   1999; Pradhan et al. 2006; Pelegri et al. 2006), but also on the SST variation over the

11   domes. In particular, the Guinea Dome plays a critical role on the seasonal-phase locking of

12   the interannual variations of the northern tropical Atlantic SST (Doi et al 2010, Fig. 18).

13   Although most studies on the Atlantic climate focused on the atmospheric forcing or the sea

14   surface field, considering the roles of ocean upwelling and stratification variations in

15   climate models is important for understanding tropical Atlantic climate modes (Doi 2009)

16   and hurricane intensity (Lloyd and Vecchi 2011).

17   Climate conditions over the tropical Atlantic Ocean have to be simulated well in

18   climate models for accurate prediction of not only the Atlantic basin, but also the global

19   climate (e.g. Stockdale et al. 2006). However, many coupled GCMs suffer from serious

20   biases in the tropical Atlantic (Davey et al. 2002). In particular, almost all CMIP3 (Coupled

1 Model Intercomparison Project; Meehl et al. 2007) climate models for the

2 Intergovernmental Panel on Climate Change Fourth Assessment Report (IPCC-AR4) show

3 warm SST biases in the eastern equatorial Atlantic and produce a zonal SST gradient along

4 the Atlantic equator with opposite sign to observations (Richter and Xie 2008). The lack of

5 the cold tongue in the equatorial Atlantic will be one reason why many coupled GCMs fail

6 to simulate and predict the Atlantic Niño (Stockdale et al. 2006). Richter and Xie (2008)

7 showed that the origin of the biases is in the anomalously weak trade winds along the

8 equator, which are associated with the ITCZ being displaced anomalously southward in

9 boreal spring. Richter et al. (2011) suggests the surface wind errors were partially due to

10 deficient precipitation over equatorial South America and excessive precipitation over

11 equatorial Africa. Recently, the University Tokyo Coupled Model (Tozuka et al. 2006) was

12 able to successfully simulate the zonal gradient of the annual mean SST (Doi et al. 2010).

13 Interestingly, the model's ability to simulate this feature depends on deep convection

14 scheme used (Tozuka et al. 2011).

15   In this paper, we investigate how increasing resolution can influence some biases

16 in tropical Atlantic climate conditions by comparing between a fully coupled ocean-

17 atmosphere climate model with a new high resolution climate model derived from it. This

18 paper is organized as follows. In section 2 brief descriptions of coarse and high resolution

19 coupled climate models are given. In section 3 the annual mean feature of SST and rainfall

20 in two models are investigated. We explore the seasonal cycle in section 4 and the

1 interannual variation in section 5 for two models and observation. In particular, we discuss

2 the seasonal phase-locking of the interannual variation in the northern tropical Atlantic SST

3 in section 5. The final section is used for summary and discussions.

4

5 **2. Models and observational datasets**

6

7 *a. GFDL-CM2.1*

8

9 The detailed formulations of the Climate Model version 2.1 developed at the

10 Geophysical Fluid Dynamics Laboratory (CM2.1) are described by Delworth et al. 2006,

11 Gnanadesikan et al. 2006, Stouffer et al. 2006, and Wittenberg et al. 2006. CM2.1 was part

12 of the CMIP3 model comparison which contributed to the IPCC AR4, and CM2.1 has been

13 shown to perform quite well for many global climate metrics (Knutson et al. 2006; Russell

14 et al. 2006). CM2.1 is also the basis of experimental seasonal to decadal forecast systems in

15 GFDL (Zhang et al. 2007). The oceanic component is based on the Modular Ocean Model

16 version 4 (MOM4) code (Griffies et al. 2005). The horizontal resolution is 1° longitudinal

17 and 1° latitudinal with enhanced tropical resolution (1/3° within 10° of the equator). There

18 are 50 vertical levels and the vertical grid spacing is a constant 10m over the top 220m.

19 Isopycnal mixing of tracers and layer thickness is based on the formulation by Gent and

20 McWilliams (1990), Griffies et al. (1998), and Griffies (1998). The mixed-layer is

1 represented by the K-profile parameterization (KPP) vertical mixing (Large et al. 1994).

2 The shortwave penetration depends on prescribed spatio-temporally varying chlorophyll

3 (Sweeney et al. 2005).

4   The atmospheric component is the AM2.1 atmosphere model (GAMDT 2005),

5 which consists of a finite volume dynamical core (Lin 2004) with 24 vertical levels, 2°

6 latitude by 2.5° longitude grid spacing, K-profile planetary boundary layer scheme (Lock et

7 al. 2000), and relaxed Arakawa-Schubert convection (Moorthi and Suarez 1992). The

8 coupled simulation is initialized from observed climatological oceanic condition at year 1

9 (Delworth et al. 2006) and then integrated subject to 1990 values of trace gases, insolation,

10 aerosols, and land cover. This radiative forcing yields a present-day control experiment.

11 The atmosphere, ocean, land and sea ice exchange fluxes every two hours and no flux

12 adjustments are employed. We have calculated monthly climatologies by averaging model

13 monthly mean output for the 300 years. Then, we define anomaly fields as deviations from

14 the monthly mean climatologies, after removing the decadal variability using an eight-year

15 running mean filter.

16

17 *b. GFDL-CM2.5*

18

19   GFDL-CM2.5 is a new high-resolution model version that derives closely from

20 GFDL-CM2.1 (Delworth et al. 2011). The oceanic component of CM2.5 uses a 0.25°

1   horizontal resolution of MOM4p1 in the tropics with the z* vertical coordinate (Griffies

2   2010), which varies from 25km near the tropics to 9km in polar regions. It is similar to the

3   oceanic component of CM2.4 model of Farneti et al. (2010). It is coupled to a 50km

4   horizontal resolution atmosphere model with 32 vertical levels on a cubed sphere grid. The

5   ocean model does not contain a parameterization for mesoscale eddy mixing. The advective

6   scheme has been modified to yield substantially lower numerical diffusion, and a

7   substantially smaller explicit viscosity than CM2.1 is employed. CM2.5 is initialized and

8   forced in similar fashion to CM2.1. We used CM2.5 monthly mean outputs for 280 years

9   with 1990 radiative forcing. The monthly averaged climatology and interannual anomaly

10   are calculated as the same manner in CM2.1.

11

12   *c. Observational datasets*

13

14   For comparison of the model simulations with observations, we use the Extended

15   Reconstructed SST version 3 (ERSSTv3; Smith et al. 2008), the Hadley Center SST

16   (HadISST; Rayner et al. 2003), the NCEP/NCAR reanalysis data (Kalnay et al. 1996),

17   ECMWF 40-year reanalysis data (ERA40; Simmons and Gibson 2000), and Objectively

18   Analyzed air-sea Fluxes (OAFlux; Yu et al. 2006) as observational datasets. Monthly

19   climatologies are calculated by averaging monthly observational data for 1960-2001, and

20   then interannual anomalies are defined as deviations from the monthly mean climatologies

1   after subtracting the eight-year running mean values. Since the OAFlux project provides

2   only latent and sensible heat fluxes in this epoch, the turbulent enthalpy fluxes of the

3   OAFlux are combined with the radiative fluxes from the NCEP/NCAR reanalysis data

4   (OAFlux-N), and with the ERA 40 reanalysis data (OAFlux-E). For precipitation data,

5   Climate Prediction Center Merged Analysis of Precipitation dataset (CMAP; Xie and Arkin

6   1997) and Global Precipitation Climatology Project dataset (GPCP; Adler et al. 2003) are

7   used for 1979-2001. The observed mixed-layer depth is estimated from the monthly

8   climatology of the World Ocean Atlas 2005 data (WOA05; Locarnini et al. 2006), as the

9   depth at which the potential density becomes 0.125 kg m^{-3} larger than the surface density, as

10   used by Levitus (1982). Also, we use 1° monthly gridded analysis of Coupled Ocean Data

11   Assimilation (CDA; Zhang et al. 2007) from 1960-2001 to explore oceanic state. For

12   satellite cloud amount data, the International Satellite Cloud Climatology Project D2

13   dataset (ISCCP; Rossow et al. 1991) is used for 1984-2001.

14

15   **3. Annual mean**

16

17   We begin by exploring the annual mean fields of the tropical Atlantic SST and

18   rainfall in observational estimates and the two GCMs (Figs. 1 and 2). The SST near the

19   northern South America coast is colder by about 1°C in CM2.1 than the observational SST

20   estimates of ERSSTv3 and HadISST. This bias is reduced in CM2.5, likely due to the more

1   reasonable simulation of the Brazil current and the eddy activity in this area from increased

2   resolution. Over the northern tropical Atlantic CM2.1 has a cold SST bias of about 1.5°C,

3   and over the eastern equatorial region CM2.1 has a warm bias of about 2.5°C. These SST

4   biases are not improved in CM2.5. In fact, the eastern equatorial SST is about 0.5°C

5   warmer in CM2.5 than that in CM2.1. Associated with the warm SST bias, the mixed-layer

6   depth in the southeastern tropical Atlantic is deeper than observations by 10m in CM2.1

7   and CM2.5 (figure not shown). The warm SST bias over the eastern equatorial region is

8   shown in almost all CMIP3 climate models, and originates from a weak easterly wind bias

9   in boreal spring (Richter and Xie 2006; Richer et al. 2010). As shown in Table 1a, the

10   easterly trade wind stress along the equator in CM2.1 is only 25% of the observed wind

11   stress in boreal spring. This bias in boreal spring trade wind is partially reduced in CM2.5,

12   but the simulated easterly is still only half that observed. The southerly winds in the

13   southeastern tropical Atlantic are also much weaker in CM2.1 and CM2.5 than that in

14   observation (Table 1b). The southerly wind stress in CM2.1 is only 20% of the observed

15   wind stress. This bias somewhat reduced in CM2.5, but not sufficiently as CM2.5 captures

16   only 30% of the observed wind stress. The meridional wind stress biases in these two

17   models may also contribute to the SST bias since the southerly winds induce cold upwelled

18   water along the West African coast in the South Hemisphere, which extends westward by

19   advection and Rossby wave propagation, and cools the eastern equatorial SST (Philander

20   and Pacanowski 1981).

1   The annual mean precipitation field is substantially improved in CM2.5 relative

2   to in CM2.1, although the rainfall associated with the marine Atlantic ITCZ in 50°-20°W is

3   overestimated in CM2.5. Both CM2.1 and CM2.5 tend to overestimate tropical

4   precipitation (Delworth et al. 2011). CM2.5 simulates the reasonable rainfall over the

5   northern South America, while CM2.1 shows a deficient rainfall there compared to the

6   observations (Figs 1, 2 and Table 1b). The Congo basin rainfall is well simulated in CM2.1

7   and CM2.5 (Table 1d). Given the results of Richter et al. (2011), we expect some

8   improvement of the equatorial zonal winds and SST from improving the precipitation

9   pattern. The winds are, indeed, marginally improved in CM2.5. However, this is not

10   sufficient to correct the mean state SST bias.

11

12   **4. Mean seasonal cycle**

13

14   Horizontal maps of the standard deviation of the monthly climatology of tropical

15   Atlantic SST are shown in Fig. 3. In observational estimates, large seasonal variations

16   appear in three areas: the northern tropical Atlantic, the equatorial region, and the Angola-

17   Benguela Area. The overall location of these features is reasonably simulated in CM2.1 and

18   CM2.5, although some differences are found in each region. In the northern tropical

19   Atlantic, CM2.1 shows larger seasonal variation of SST, which extends further westward

20   than observed. This bias is reduced in CM2.5. In the equatorial region, both models

13

1   overestimate the amplitude of seasonal cycle of SST. In the Angola-Benguela Area, CM2.1

2   shows larger seasonal variation of SST than observed, while CM2.5 shows much larger

3   variation trapped near the West African coast.

4   To understand the mechanisms behind the seasonal cycle in those three areas, we

5   explore a diagnostic mixed-layer heat budget (Appendix 1). First, we focus on the Northern

6   Tropical Atlantic (NTA: 35°-18°W, 5°-20°N). As shown in Fig. 4, the seasonal cycle of the

7   SST in the NTA can be largely understood in terms of the surface enthalpy flux contribution.

8   In boreal spring, the surface enthalpy flux warms the SST, although we have large

9   discrepancy among the observational datasets: NCEP/NCAR reanalysis data, ERA40

10   reanalysis data, and OAFlux data. The discrepancy is caused by shortwave radiation and

11   latent flux since the longwave radiation and sensible flux are only less 10% of the total

12   discrepancy. Therefore, it is difficult to constrain the observed contribution from ocean

13   dynamics in boreal spring. However, this ambiguity is not apparent in boreal summer; the

14   warming tendency of SST in summer is mainly due to the surface enthalpy flux, but cooling

15   by ocean dynamics also plays an important counteracting role. This is consistent with the

16   observational study of Yu et al (2006). The cooling tendency from ocean dynamics in

17   boreal summer arises from a subsurface doming of the thermocline in the northeastern

18   tropical Atlantic, known as the Guinea Dome (or the Dakar Dome; Mazeika 1967). The

19   Guinea Dome develops from boreal spring through summer from the Ekman upwelling

20   associated with the seasonal meridional migration of the ITCZ (Siedler et al. 1992;

1   Yamagata and Iizuka 1995; Doi et al. 2009; Doi et al. 2010). Fig. 5 shows the summer field

2   of wind stress, Ekman upwelling, and ocean stratification around mixed-layer depth. In the

3   observational and assimilated estimates, the Guinea Dome is climatologically located in

4   10°-15°N, 35°-20°W, while the simulated dome in CM2.1 is four times stronger than

5   observation, and located further north by 3°N, and extends further westward. These biases

6   in CM2.1 are associated with the stronger Ekman upwelling over the Guinea Dome region

7   arising from an excessive northward migration of the ITCZ and a stronger West African

8   Monsoon than observed. Fig. 6 shows the coupled meridional migration of the ITCZ,

9   through rainfall, SST, and Ekman upwelling zonally averaged in 50°-20°W. In boreal

10   summer, the simulated ITCZ in CM2.1 located around 13°N, while the observation shows

11   the ITCZ around 9°N. The large northward migration of the ITCZ in CM2.1 causes the

12   strong bias in the Ekman upwelling over the Guinea Dome in boreal summer. Therefore,

13   CM2.1 overestimates the cooling by the ocean dynamics in summer, as shown in Fig. 4c.

14   These biases are greatly reduced in CM2.5 (Figs 4 and 5).

15   Crucial to the improvement in the Guinea Dome, and associated ocean dynamical

16   cooling in CM2.1 was an improved meridional migration and strength of the ITCZ (Fig. 6).

17   The spring location of the simulated ITCZ in CM2.5 is 3°S and its summer location is 9°N,

18   which is consistent with observed. In late autumn and early winter, the cooling by the net

19   surface enthalpy flux is stronger in both models than that in any observational dataset, a

20   bias that is largely due to latent heat flux. The net shortwave radiation follows total cloud

15

1   amount. Complicating our analysis it the large observational uncertainty between the

2   various estimates of low clouds and shortwave radiation (Figs. 4g, h). However, the

3   apparent bias in CM2.1 for a weak bias of downward shortwave radiative flux in boreal

4   summer arising from large cloud amount appears reduced in CM2.5.

5   Next, we discuss the equatorial region (ATL3: 20°W-0°W, 3°S-3°N). The ATL3

6   index is also used in Zebiak (1993). The cold tongue in this region develops from boreal

7   spring through summer (Fig. 7). Ocean dynamics is the main contributor to this cooling

8   tendency of the mixed-layer temperature. Both the cold tongue cooling and ocean

9   dynamical contribution are underestimated in CM2.1 and CM2.5, with the ocean dynamical

10   cooling being about 50% less than the observational estimates from the NCEP/NCAR,

11   OAFlux-N, and OAFlux-E data (Fig. 7c). These biases in the ocean dynamical contribution

12   in two models arise from the deep mixed-layer depth and the weak equatorial upwelling

13   that is driven by the excessive relaxation of the zonal wind stress along the equator in

14   boreal spring, as discussed in Section 2. Also, the warming tendency by the net surface

15   enthalpy flux during boreal summer is underestimated in CM2.1 and CM2.5, which is due

16   to strong latent heat loss from ocean and weak downward shortwave radiation (Figs 7e, f,

17   and g). These biases arise from the warm SST bias and excessive cloud in two models. As

18   shown in Fig.7h, total cloud amount in summer is larger in CM2.1 and CM2.5 than

19   observed. During boreal winter, the warming tendency by the net surface enthalpy flux

20   contribution is overestimated in both models, which is also mainly due to strong downward

16

1   shortwave radiation arising from deficient cloud.

2   For the Angola-Benguela Area (ABA: 0°E-20°E, 25°-5°S), the observed and

3   modeled SST cools from April through August largely due to the net surface enthalpy flux

4   changes (Fig. 8a). In both CM2.1 and CM2.5, the net surface enthalpy flux out of the ocean

5   is much stronger than observed (Fig. 8e), mainly due to the biases in the latent heat flux due

6   to the warm SST bias (Fig. 4i). However, the cooling effect of this excessive surface

7   enthalpy flux is underestimated in CM2.1 and CM2.5, because the mixed-layer depth in

8   CM2.1 and CM2.5 is deeper than that in observations, as discussed in Section 2. In austral

9   late winter, the Angola Dome matures in observational estimates (Yamagata and Iizuka

10   1995; Doi et al. 2007), but CM2.1 and CM2.5 fail to simulate the strong doming in 15°-5°S,

11   0-12°E (Fig. 5). Therefore, ocean dynamical cooling in austral late winter is weaker in

12   CM2.1 and CM2.5 than observational estimates (Fig. 8c). From October through March,

13   the observed and modeled SST is warmed by the surface enthalpy flux change. In austral

14   summer we have large differences between the downward shortwave radiation in the

15   NCEP/NCAR reanalysis data and that in the ERA-40 reanalysis data, likely due to

16   ambiguity of cloud.

17   Fundamental to and interacting with the seasonal SST variations over the tropical

18   Atlantic is the associated meridional migration of the ITCZ. The improvement in the ITCZ

19   variation in CM2.5 is reflected in its representation of the rainfall over the Sahel and

20   northern South America (Fig. 9). The Sahel rainfall has its peak in boreal summer

1 associated with the West African Monsoon. Although this feature is overestimated by about

2 40% in CM2.1, but in CM2.5 it is very similar to observations. In northern South America,

3 CM2.1 shows the dry biases, in particular during boreal summer. The simulated summer

4 rainfall in CM2.1 over northern South America is only 20 % in observations. However, the

5 CM2.5 simulation is much more reasonable.

6

7 **5. Interannual variation**

8

9 The horizontal maps of the standard deviation of the interannual SST variation

10 are shown in Fig.10. As in the seasonal SST variation, the interannual variability is large in

11 three regions, each of which has strong seasonal phase-locking of the variability (Fig. 11).

12 Thus, these interannual variations in the tropical Atlantic can be interpreted as a modulation

13 of the seasonal cycle. In observations, the variability is phase-locked to boreal

14 spring/summer, while the models shows a large variability for all three regions not only in

15 boreal spring/summer, but also in boreal autumn.

16 We begin by exploring the seasonal phase-locking of the interannual variations of

17 SST averaged in the NTA (Fig. 11a). The observational SST anomaly develops from

18 February, reaches its peak in April, and decays abruptly from May through September. The

19 observational SST anomaly in September is about 40% smaller than that in April. CM2.1

20 successfully simulates the developing phase from early winter through boreal spring.

1 However, the SST anomaly keeps warming through March-May, and the decay from June

2 through August is weak in CM2.1 compared to observations. As a result, the interannual

3 variation of the NTA SST in August is 65% stronger in CM2.1 than that in observations.

4 This bias in the seasonal phase-locking of the interannual variation of the NTA SST in

5 CM2.1 is reduced in CM2.5, although the peak in CM2.5 appears one month earlier than

6 the observational peak. As seen by the horizontal mapping of the standard deviation in the

7 early hurricane season of August (Figs. 10f), the bias of CM2.1 is largest in the Guinea

8 Dome region. Since many of the climatic impacts of TNA interannual variability are

9 seasonally phase-locked (e.g. Sahel rainfall, West African monsoon, Atlantic hurricane, etc),

10 this bias in the seasonal phasing of the interannual variations of SST over the Guinea Dome

11 region in CM2.1 could represent a serious deficiency. Therefore, we aim to understand its

12 causes in CM2.1, and why this bias is improved in CM2.5.

13   We explore a composite analysis to help understanding the mechanism of the

14 seasonal phase locking of interannual variations of SST in the NTA. We construct a

15 composite by averaging, based on selecting warm (cold) SST years in the NTA, when the

16 interannual SST anomaly in the NTA exceeds one standard deviation during the mature

17 season. The details are shown in Table 2. We have about 1.5 year per decade as a composite

18 year in observations and models.

19   We begin to discuss the developing phase in the warm years of the northern

20 tropical Atlantic. In observations, the SST anomaly in the NTA warms from early winter

1   through May and the warming tendency is strongest in February (Fig. 12a), mainly due to

2   the surface enthalpy flux contribution. This is well simulated in both CM2.1 and CM2.5,

3   although in CM2.1 the maximum warming tendency is found in March, while in CM2.5 it

4   is around January. We note that interannual variations of surface enthalpy flux contribution,

5    $\frac{Q - q_{sw}}{\rho C_p H_{mix}}$ in Appendix-1, includes not only interannual variations of surface enthalpy flux,

6   but also interannual variations of mixed-layer depth (e.g. Morioka et al 2010; 2011).

7   However, we have confirmed that interannual variations of mixed-layer depth do not

8   contribute to the surface enthalpy flux term over the northern tropical Atlantic in boreal

9   spring (figure not shown). All observational datasets, CM2.1, and CM2.5 show latent heat

10   flux anomaly as the dominant term in the net surface enthalpy flux anomaly (Fig.11b). As is

11   shown in Fig.13 through the composite evolution of the net surface enthalpy flux, latent

12   heat flux, and wind stress anomalies in February, the warming mechanism is consistent

13   with the wind-evaporation-SST (WES) positive feedback (Xie 1999) associated with the

14   ITCZ migration: 1) an anomalously northward migration of the ITCZ causes the

15   southwesterly wind anomaly in the northern tropics and weaker trade winds, 2) this results

16   in less evaporation and thus suppressed latent heat loss from ocean, leading to warmer SST

17   in the northern tropical Atlantic. 3) The outcome is the further northward migration of the

18   ITCZ. The dominance of this mechanism in the growth of anomalies has been discussed in

19   previous works (Carton et al. 1996; Chang et al. 1997; Xie 1999; Huang and Shukla 2005;

20   Hu et al. 2008). Both CM2.1 and CM2.5 reasonably capture the WES feedback (Fig. 13),

1 although some biases are found in two models. In CM2.1, the strongest warming area is

2 about 4° southward of that in observations. This may be due to the southerly ITCZ location

3 bias during boreal winter in mean climatology, as discussed in section 4. The WES

4 feedback characteristics in CM2.5 are more realistic than those in CM2.1.

5 While the essence of the spring development mechanism is successfully

6 reproduced in both CM2.1 and CM2.5, the summer decay mechanism is incorrectly

7 represented in CM2.1. In observations, the SST anomaly in the NTA starts to decay from

8 May through September. The NCEP/NCAR reanalysis, OAFlux-N, and OAFlux-E datasets

9 show that the ocean dynamical contribution plays an important role on the summer decay

10 (Fig. 12a, Table 3). It has been suggested that the ocean dynamical cooling counteracts the

11 warming by the WES feedback and provides an important negative feedback that helps to

12 terminate warm events (Joyce et al 2004; Lee and Wang 2008; Doi et al. 2009; Doi et al.

13 2010; Mahajan et al. 2010). However, CM2.1 fails to simulate the cooling effect by the

14 ocean dynamical contribution and shows the warming tendency by the ocean dynamical

15 contribution. Therefore, the peak season of the SST anomaly moves from boreal spring into

16 early summer and the warm SST anomaly is sustained through late summer in CM2.1. The

17 bias in the ocean dynamical contribution is reduced in CM2.5

18 Why does CM2.1 fail to simulate the decay mechanism by the ocean dynamical

19 contribution in boreal summer? We explored the diagnostic mixed-layer heat budget

20 anomaly in the NTA (Eq. A2 in Appendix), and found that CM2.1 cannot capture the

1 negative feedback associated with the Guinea Dome. As discussed above, the WES positive

2 feedback in the development mechanism amplifies an anomalously northward migration of

3 the ITCZ, which leads to the positive wind stress curl anomaly and strong Ekman

4 upwelling anomaly over the Guinea Dome region. Therefore, the strong upwelling plays an

5 important role on the termination of the warm SST anomaly in the NTA through

6 entrainment (schematic diagram: Doi et al. 2010, Fig. 18). Observational and assimilation

7 datasets show the Ekman upwelling anomaly over the climatological Guinea Dome region

8 arising from the northward ITCZ migration (Fig. 14a-b). However, in CM2.1, the Ekman

9 downwelling anomaly is dominant over the Guinea Dome region (Fig. 14c). The

10 disagreement of the wind-induced vertical velocity over the Guinea Dome between

11 observations and CM2.1 is due to the seasonal further northward migration of the ITCZ in

12 CM2.1 from boreal spring to summer, as shown in section 4. The WES feedback amplifies

13 the bias in the seasonal northward ITCZ migration in CM2.1, and results in the Ekman

14 upwelling anomaly further north around 16°-21°N, while the Ekman downwelling anomaly

15 over the strong climatological doming in CM2.1. The downwelling anomaly over the

16 Guinea Dome warms the SST significantly in boreal summer. In fact, the vertical

17 entrainment contribution arising from the entrainment rate anomaly, $(W_{ent})' * \overline{\left(\frac{T_{mld} - T_d}{H_{mld}}\right)}$ (Appendix

18 2), can explain about 80% of the warming tendency by the ocean dynamics in CM2.1

19 during boreal early summer (Table 3). Since the Ekman downwelling anomaly also

20 weakens the doming of thermocline, the anomalous vertical entrainment effect arising from

22

1   the ocean stratification anomaly, $(\overline{W_{ent}}) * \left(\frac{T_{mld} - T_d}{H_{MLD}}\right)'$, partially contributes to the warming

2   tendency by the ocean dynamics in CM2.1. This entrainment error contributes to

3   maintaining the warm SST anomaly over the Guinea Dome through boreal summer in

4   CM2.1. This incorrect oceanic feedback associated with the Guinea Dome in CM2.1 is

5   improved in CM2.5 in part because the seasonal meridional migration of the ITCZ is well

6   simulated. Recovering the correct seasonal meridional migration of the Atlantic ITCZ is

7   key not only for the mean seasonal cycle, but also for the seasonal phase-locking of the

8   interannual variations of the NTA SST.

9   The precipitation field is also changed in the warm NTA SST years. CM2.1

10   shows excessive summer rainfall in the Sahel, due to the sustained warm NTA SST

11   anomaly in boreal summer (Fig. 15). In northern South America, CM2.1 shows much less

12   rainfall in boreal spring, due to the anomalously northward migration of the ITCZ

13   associated with the warm NTA SST. Observations and CM2.5 do not show the significant

14   rainfall anomaly over the Sahel and northern South America. The large meridional

15   migration of the ITCZ in CM2.1 would result in unrealistically large variations in

16   simulating the Sahel rainfall and the northern South America rainfall, although we have

17   uncertainty because of lack of observational datasets.

18   The cold years of the NTA SST can be explained by using similar mechanisms of

19   opposite sign to the warm years. Therefore, relevant figures are not shown in this paper.

20   The cold SST anomaly in the NTA is developing from early boreal winter through spring.

23

1 The cooling tendency is mainly due to the surface enthalpy flux contribution associated

2 with the WES feedback: an anomalously southward migration of the ITCZ arising from the

3 cold SST anomaly in the NTA causes the northeasterly wind anomalies and stronger trade

4 winds in the NTA. This results in excessive evaporation and enhanced latent heat loss from

5 ocean, and amplified the cold SST anomaly in the NTA. This development mechanism is

6 simulated well in CM2.1 and CM2.5. In the summer decay phase, the cold SST anomaly in

7 the NTA starts to decay from May arising from the warming effect by both the surface

8 enthalpy flux contribution and the ocean dynamical contribution in observations. In

9 particular, the observational estimate by the NCEP/NCAR reanalysis OAFlux-N datasets

10 show the important warming tendency by the ocean dynamics in May-July. However,

11 CM2.1 and CM2.5 fail to simulate this oceanic warming effect. By the diagnostic mixed-

12 layer heat budget analysis in the NTA, we found that the disagreement of ocean dynamics

13 in two models is mainly due to the wind-induced vertical velocity fields. Although the

14 observations show the Ekman downwelling anomaly over the Guinea Dome region, CM2.1

15 and CM2.5 show the Ekman upwelling anomaly over the dome region due to the

16 unrealistically large meridional migration of the ITCZ. The unrealistic large meridional

17 migration of the ITCZ in CM2.1 also has an impact on the precipitation field. CM2.1 shows

18 less summer rainfall in the Sahel, while, in northern South America, CM2.1 shows

19 excessive rainfall in boreal spring.

20   In the equatorial Atlantic (ATL3), the interannual variation of observed SST has

1   its peak in boreal summer. This captures the Atlantic Niño (Zebiak, 1993; Carton and

2   Huang 1994). CM2.1 and CM2.5 show that the mature season is boreal summer as in

3   observations, but their peaks move to 1 month later and show about 2 times stronger than

4   that in observations. In the Angola-Benguela Area (ABA), the observations show the

5   interannual variation of SST matures in boreal spring. This is known as the Benguela Niño

6   (Florenchie et al 2003). Unfortunately, CM2.1 and CM2.5 fail to simulate the seasonal

7   phase-locking of the interannual variations of SST there. The simulated peak seasons in

8   CM2.1 and CM2.5 shift to boreal summer as in ATL3. These large disagreements for the

9   seasonal phase-locking of the interannual variations of SST in ATL3 and ABA in two

10   models are probably due to the large biases in the mean state and seasonal climatology in

11   ATL3 and ABA, as discussed in the previous sections. Although these regions are

12   interesting, in this paper we have focused on the bias in the NTA, because the high

13   resolution CM2.5 successfully reduced the bias in CM2.1.

14

15   **5. Discussions and summary**

16

17   Using output from the "1990 Control" simulations of two coupled GCMs (CM2.1

18   and the high-resolution CM2.5), the tropical Atlantic biases in the mean state, the seasonal

19   cycle, and the interannual variations were investigated. Many aspects of the simulation are

20   improved in CM2.5–yet others are not. The mean seasonal cycle of the rainfall over the

1   Sahel and the northern South America are well simulated in CM2.5, while CM2.1 shows

2   the excessive rainfall over the Sahel and the deficient rainfall over northern South America

3   particularly in boreal summer. The better simulation of rainfall in CM2.5 arises from a

4   more realistic meridional migration of the simulated ITCZ, while the meridional migration

5   of the ITCZ in CM2.1 is larger than that in observations. The biases in the meridional

6   migration of the ITCZ in CM2.1 involve coupled feedbacks, and are evident in both SST

7   and Ekman upwelling velocity. The improved meridional migration of the ITCZ in CM2.5

8   is a key factor for the better simulation of not only the West African Monsoon, but also the

9   Guinea Dome. The Guinea Dome develops from late spring through summer and matures

10   in autumn driven by the wind-induced Ekman upwelling associated with the northward

11   migration of the ITCZ. Although both CM2.1 and CM2.5 capture the seasonal variations of

12   the Guinea Dome. CM2.5 better reproduces the local wind-induced Ekman upwelling and

13   the oceanic stratification around the mixed-layer depth over the Guinea Dome in boreal

14   summer, while the Guinea Dome in CM2.1 is much stronger and moves further northward

15   than that in observations. Since entrainment cooling plays an important role on the seasonal

16   variation of the SST over the Guinea Dome from boreal summer through autumn, the

17   summer cooling tendency of the northern tropical Atlantic SST by the ocean dynamics is

18   stronger in CM2.1 than that in observations, while this ocean dynamical contribution over

19   the Guinea Dome is well simulated in CM2.5. These coupled biases strongly influence the

20   seasonal dependence of the interannual variations of SST in the northern tropical Atlantic.

1   The interannual SST anomaly in the northern tropical Atlantic develops from

2   early boreal winter through spring, and reaches the maximum in April in observations. This

3   is driven by the Wind-Evaporation-SST (WES) positive feedback mechanism connected to

4   the ITCZ meridional migration; an anomalously northward migration of the ITCZ causes

5   the southwesterly wind anomalies and the weak trade winds in the northern tropical

6   Atlantic. This leads to weak evaporation and suppressed latent heat loss from ocean, which

7   warms the SST in the northern tropical Atlantic. This development mechanism is

8   successfully simulated in both CM2.1 and CM2.5, although the area of strongest warming

9   in CM2.1 is shifted southward compared to that in observations. This is because the ITCZ

10   simulated in CM2.1 is located about 3° southward from the observed ITCZ in the mean

11   climatology of February.

12   The mechanism for summer decay of NTA interannual variability is not well

13   simulated in CM2.1. The modeled maximum of the SST anomaly in the northern tropical

14   Atlantic appears one month later and the summer decay is 65% weaker in CM2.1 than that

15   in observations. Therefore, the interannual NTA SST anomalies in CM2.1 remain through

16   August. This seasonal bias in interannual variability may be behind a reduction in the short-

17   lead seasonal prediction skill for Atlantic hurricane with CM2.1 (Vecchi et al. 2011). It

18   could also influence predictions of the Sahel rainfall changes associated with the summer

19   West African monsoon. The bias in the summer decay phase of the interannual SST

20   anomaly in CM2.1 is mainly due to the ocean dynamical contribution by the Guinea Dome.

1   In observations, the warm SST anomaly over the subsurface Guinea Dome significantly

2   decays by the negative feedback linked with the Guinea Dome (Doi et al. 2010): the

3   anomalously northward migration of the ITCZ associated with the warm SST anomaly in

4   the northern tropical Atlantic leads to the cyclonic wind stress curl anomaly, and thus the

5   Ekman upwelling anomaly over the Guinea Dome region. It plays a critical role on the

6   summer decay of the warm SST anomaly through entrainment cooling (schematic diagram

7   is shown in Fig. 16a). However, CM2.1 fails to simulate this negative feedback. The large

8   northward migration of the modeled climatological ITCZ leads to the Ekman upwelling

9   anomaly in the further north of the Guinea Dome region, and the Ekman downwelling

10   anomaly just over the Guinea Dome. Since the climatological doming is anomalously

11   stronger in CM2.1 than that in observation, the Ekman downwelling anomaly over the

12   Guinea Dome sustains the warm SST anomaly there as an incorrect positive feedback (Fig.

13   16b). CM2.5 successfully reproduces the seasonal phase-locking of the interannual

14   variations of the northern tropical Atlantic SST. This is due to the realistic climatological

15   meridional migration of the ITCZ in CM2.5, which generates the Guinea Dome reasonably

16   and leads to the realistic decay of the interannual anomaly of the northern tropical Atlantic.

17   In this paper, we focused on the present-day simulations, but we note that the seasonal

18   phase-locking of the northern tropical Atlantic shows the interesting responses by the

19   Climate Change. In two-times CO_2 increase experiment, the peak of interannual variation

20   of the northern tropical Atlantic SST moved to boreal early summer (Doi et al. 2011, *to be*

1   *submitted to J. Climate*).

2   It appears that the increased resolution and other changes in parameterizations in

3   CM2.5 have acted to reduce some biases in the meridional migration of the ITCZ. CM2.5

4   successfully reproduces the seasonal cycle of the rainfall over the Sahel and the northern

5   South America, the Guinea Dome, and the seasonal phase-locking of the interannual

6   variations of the northern tropical Atlantic. Because of this, we hypothesize that CM2.5

7   may exhibit better prediction skill of the northern Atlantic climate conditions than CM2.1.

8   However, the differences between CM2.5 and CM2.1 (including resolution) were not

9   sufficient to reduce the SST biases in the eastern equatorial region and Angola-Benguela

10 Area, the former being a ubiquitous bias that is found in almost all IPCC-AR4 models

11 (Richter and Xie 2008). The seasonal cycle and the interannual variations of SST in these

12 two areas are stronger in both models than in observations. In particular, neither model can

13 simulate the seasonal phase-locking of the interannual variations of SST over the Angola-

14 Benguela Area. Therefore, neither model realistically simulates the Atlantic Niño and the

15 Benguela Niño, which are major climate modes in the tropical Atlantic. As shown in Table

16 1, the weak trade winds along the equator and the weak southerly winds along the

17 southwestern African coast are likely causative factors for these biases. Since biases may

18 arise and be amplified by air-sea-land coupled process, it is difficult at this stage to specify

19 the ultimate origin of the wind biases. However, the results of Tozuka et al. (2011) indicate

20 that changes in the deep convection schemes could be a key to reduce the biases in the wind

29

1   field associated with the ITCZ, the Walker circulation, the sea level pressure and the

2   precipitation over the Amazon and the Sahel. We speculate that the problems are mostly

3   related to atmospheric physics in AGCM. Sensitivity experiments for reducing the tropical

4   Atlantic biases are being conducted as part of GFDL's research program.

5   In this paper, we have focused on the tropical Atlantic basin. However,

6   uncertainty still remains as to the role of the Pacific, the mid-latitude Atlantic, the tropical

7   southern Atlantic on climate conditions in the Atlantic (see reviews by Xie and Carton

8   2004; Chang et al. 2006). In particular, Czaja (2004) suggested that the seasonal

9   dependence of the interannual variability in the northern tropical Atlantic is a reflection not

10 only of local air-sea coupling, but also the remote forcing by the North Atlantic Oscillation

11 and the ENSO. Although ENSO is stronger in CM2.1 than that in observations (Wittenberg

12 et al. 2006), this bias is partially reduced in CM2.5. Exploring the relation between the

13 tropical Atlantic and other basins is also underway.

14

Appendix: Mixed-layer heat budget analysis

We explore the diagnostic bulk mixed-layer heat budget:

$$\frac{\partial T_{mix}}{\partial t} = \frac{Q - q_{sw}}{\rho C_p H_{mix}} + ocean\ dynamics\ contribution\ . \tag{A1}$$

Here, T_{mix} is the mixed-layer temperature, a proxy for SST, ρ is the typical sea water density (1025 kg m^{-3}), C_p is the typical heat capacity of the sea water (3996 J kg^{-1} K^{-1}), and H_{mix} is the mixed-layer depth, which is calculated as the depth at which the potential density becomes 0.125 kg m^{-3} larger than the surface density, as used by Levitus (1982). The quantity Q denotes the net surface enthalpy flux, and q_{sw} is the downward solar insolation that penetrates through the bottom of the mixed-layer. Thus, the first term on the right hand side represents the influence of atmospheric thermal forcing. The ocean dynamical contribution is simply estimated by difference between rate of change of the mixed-layer temperature and the surface enthalpy flux contribution.

To understand the detailed ocean dynamical contribution in the Guinea Dome region, we explore the detailed mixed-layer heat budget:

$$\frac{\partial T_{mix}}{\partial t} = \frac{Q - q_{sw}}{\rho C_p H_{mix}} - W_{ent} \frac{T_{mix} - T_e}{H_{mix}} - \vec{U} \cdot \nabla T_{mix} + residual\ . \tag{A2}$$

The second term on the right hand side represents the oceanic cooling associated with entrainment, where W_{ent} is the entrainment rate, and T_e is the temperature of water entrained into the mixed-layer and assumed to be the temperature 5 m below the mixed-layer (e.g. Qu et al. 2001). The entrainment rate can be assumed by

31

1 $$W_{ent} = \frac{\partial H_{mix}}{\partial t} + W_{mb} + \vec{U} \cdot \nabla H_{mix} \,, \qquad\qquad (A3)$$

2 where $\dfrac{\partial H_{mix}}{\partial t}$ denotes the rate of change of the mixed-layer depth, W_{mb} is the vertical

3 velocity at the base of the mixed-layer, and $\vec{U} \cdot \nabla H_{mix}$ is the horizontal transport. If W_{ent} is

4 negative, we assume $W_{ent} = 0$. This estimation of the oceanic entrainment cooling is a well-

5 known diagnostic method (e.g. Hagos and Cook 2009). The third term, $\vec{U} \cdot \nabla T_{mix}$, represents

6 the horizontal heat transport in the mixed-layer.

7

References

Adler, R.F., and Coauthors, 2003: The version 2 Global Precipitation Climatology Project (GPCP) monthly precipitation analysis (1979-Present). *J. Hydrometeor.*, **4,** 1147-1167.

Binet, D., B. Gobert, and L. Maloueki, 2001: El Niño-like warm events in the eastern Atlantic (6°N, 20°S) and fish availability from Congo to Angola (1964-1999). *Aquat. Living Resour.*, **14,** 99-113.

Carton, J. A., and B. Huang, 1994: Warm events in the tropical Atlantic. *J. Phys. Oceanogr.*, **24,** 888-903.

Carton, J. A., X. Cao, B. S. Giese, and A. M. da Silva, 1996: Decadal and interannual SST variability in the tropical Atlantic Ocean. *J. Phys. Oceanogr.*, **26**, 1165-1175.

Chang, P., L. Ji, and H. Li, 1997: A decadal climate variation in the tropical Atlantic ocean from thermodynamic air-sea interactions. *Nature,* **385,** 516-518.

Chang, P., and Coauthors, 2006: Climate fluctuations of tropical coupled system –the role of ocean dynamics. *J. Climate*, **19,** 5122-5174.

Czaja, A., 2004: Why is North Tropical Atlantic SST variability stronger in boreal spring? *J. Climte*, **17,** 3017-3025.

Davey, M. K., and coauthors, 2002: STOIC: a study of coupled model climatology and variability in tropical ocean regions. *Climate Dyn.*, **18**, 403-420.

Delworth, T. L., and Coauthors, 2006: GFDLs CM2 global coupled climate models. Part I : Formulation and simulation characteristics. *J. Climate*, **19,** 643-674.

1   Delworth, T. L., and Coauthors, 2011: Simulated climate and climate change in the GFDL-

2   CM2.5 high-resolution coupled climate model. *Submitted to J. Climate*.

3   Doi, T., T. Tozuka, H. Sasaki, Y. Masumoto, and T. Yamagata, 2007: Seasonal and

4   interannual variation of oceanic conditions in the Angola Dome, *J. Phys. Oceanogr.,* **37,**

5   2698-2713.

6   Doi, T., T. Tozuka, and T. Yamagata, 2009: Interannual variability of the Guinea Dome and

7   its possible link with the Atlantic Meridional Mode. *Climate Dyn.*, **33**, 985-998.

8   Doi, T., 2009: Tropical Atlantic climate modes and their links with upwelling domes. Ph.D.

9   thesis, the University of Tokyo, 141 pp.

10   Doi, T., T. Tozuka, and T. Yamagata, 2010: The Atlantic Meridional Mode and its coupled

11   variability with the Guinea Dome. *J. Climate*, **23,** 455-475.

12   Dommenget, D., V. Semenov, and M. Latif, 2006: Impacts of the tropical Indian and

13   Atlantic Oceans on ENSO, *Geophys. Res. Lett.*, **33**, doi:10.1029/2006GL025871.

14   Emanuel, K., 2005: Increasing destructiveness of tropical cyclones over the past 30 years.

15   *Nature*, **436,** 686-688.

16   Farneti, R., T. L. Delworth, A. J. Rosati, S. M. Griffies, F. Zeng, 2010: The role of

17   mesoscale eddies in the rectification of the Southern Ocean response to climate change.

18   *J. Phys. Oceanogr.*, **40**, 1539–1557.

19   Folland, C. K., A. W. Colman, D. P. Rowell, M. K. Davey, 2001: Predictability of northeast

20   Brazil rainfall and real-time forecast skill, 1987–98. *J. Climate*, **14**, 1937–1958.

1   Florenchie, P., J. R. E. Lutjeharms, C. J. C. Reason, S. Masson, and M. Rouault, 2003: The

2   source of Benguela Niños in the South Atlantic Ocean. *Geophys. Res. Lett.*, **30,** doi:

3   10.1029/2003GL017172.

4   GAMDT, 2004: The new GFDL global atmosphere and land model AM2/CM2.0:

5   Evaluation with prescribed SST simulations. *J. Climate*. **17**, 4641–4673.

6   Gent, P.R., and J. C. McWilliams, 1990: Isopycnal mixing in ocean circulation models. *J.*

7   *Phys. Oceanogr.*, **20**, 150–155.

8   Gnanadesikan, A., and Coauthors, 2006: GFDL's CM2 global coupled climate models. Part

9   II: The baseline ocean simulation. *J. Climate*, **19,** 675–697.

10   Griffies, S. M., 1998: The Gent-McWilliams skew flux. *J. Phys. Oceanogr.*, **28**, 831-841.

11   Griffies, S. M., A. Guanadesikan, R. C. Pacanowski, V. D. Larichev, J. K. Dukowicz, and R.

12   D. Smith, 1998: Isoneutral diffusion in a z-coordinate ocean model. *J. Phys. Oceanogr.*,

13   **28**, 805–830.

14   Griffies, S. M., and Coauthors, 2005: Formulation of an ocean model for global climate

15   simulations. *Ocean Sci.,* **1.** 45-79.

16   Griffies, S. M., 2010: Elements of MOM4p1. *GFDL OCEAN GROUP TECHNICAL*

17   *REPORT NO. 6*, p444.

18   Hagos, S. M., and K. H. Cook, 2009: Development of a coupled regional model and its

19   application to the study of interactions between the West African monsoon and the

20   eastern tropical Atlantic Ocean. *J. Climate*, **22**, 2591–2604.

1   Hodson, D. L. R., R. T. Sutton, C. Cassou, N. Keenlyside, Y. Okumura, and T. Zhou:

2   Climate impacts on recent multidecadal changes in Atlantic Ocean Sea Surface

3   Temperature: a multimodel comparison. *Climate Dyn.*, **34,** 1041-1058.

4   Hu, Z.-Z., B. Huang, and K. Pegion, 2008: Leading patterns of the tropical Atlantic

5   variability in a coupled general circulation model. *Climate Dyn.*, **30**, 703-726.

6   Huang, B., and J. Shukla, 2005: Ocean-atmosphere interactions in the tropical and

7   subtropical Atlantic ocean. *J. Climate*, **18,** 1652-1672.

8   Joyce, T. M., C. Frankignoul, J. Yang, and H. E. Phillips, 2004: Ocean response and

9   feedback to the SST dipole in the Tropical Atlantic. *J. Phys. Oceanogr.,* **34**, 2525-2540.

10 Kalnay, E., and Coauthors, 1996: The NCEP/NCAR 40-year reanalysis project. *Bull. Amer.*

11   *Meteor. Soc.,* **77,** 437-471.

12 Knutson, T. R., and Coauthors, 2006: Assessment of Twentieth-Century Regional Surface

13   Temperature Trends Using the GFDL CM2 Coupled Models. *J. Climate*, **19**,

14   1624–1651.

15 Kossin, J. P., and D. J. Vimont, 2007: A more general framework for understanding Atlantic

16   Hurricane variability and trends. *Bull. Amer. Meteor. Soc.,* **88,** 1767-1781.

17 Kucharski, F., I.-S. Kang, R. Farneti, and L. Feudale, 2011: Tropical Pacific response to

18   20th century Atlantic warming, *Geophys. Res. Lett.,* **38**, doi:10.1029/2010GL046248.

19 Kushnir, Y., W. A. Robinson, P. Chang, and A. W. Robertson, 2006: The physical basis for

20   predicting Atlantic sector seasonal to interannual climate variability. *J. Climate*, **19,**

1   5949-5970.

2   Large, W. G., J. C. McWilliams, and S. C. Doney, 1994: Oceanic vertical mixing: A review

3   and a model with a nonlocal boundary layer parameterization. *Rev. Geophys.*, **32,** 363-

4   403.

5   Lee, S.-K. and C. Wang, 2008: Tropical Atlantic decadal oscillation and its impact on the

6   equatorial atmosphere-ocean dynamics: A simple model study. *J. Phys. Oceanogr.,* **38,**

7   193-212.

8   Levitus, S., 1982: Climatological Atlas of the World Ocean, NOAA Professional Paper 13,

9   U.S. Department of Commerce.

10   Lin, S-J., 2004: A "vertically Lagrangian" finite-volume dynamical core for global models.

11   *Mon. Wea. Rev.,* **132,** 2293-2307.

12   Lloyd, I. D., and G. A. Vecchi, 2011: Observational evidence for oceanic controls on

13   Hurricane intensity. *J. Climate,* **24**, 1138–1153.

14   Locarnini, R.A., A.V. Mishonov, J.I. Antonov, T.P. Boyer, H.E. Garcia and S. Levitus, 2006:

15   World Ocean Atlas 2005, Volume 1: Temperature. S. Levitus. *NOAA Atlas NESDIS 61,*

16   *U.S. Government Printing Office, Washington, D.C Äi0: 182*.

17   Look, A. P., A. R. Brown, M. R. Bush, G. M. Martin, and R. N. B. Smith, 2000: A new

18   boundary layer mixing scheme. Part Ⅰ: Scheme description and single-column model

19   tests. *Mon. Wea. Rev.,* **128,** 3187-3199.

20   Lu, J., and T. L. Delworth, 2005: Oceanic forcing of the late 20th century Sahel drought.

1   *Geophys. Res. Lett.*, **32**, doi:10.1029/2005GL023316.

2   Mazeika, P. A., 1967: Thermal domes in the eastern tropical Atlantic Ocean. *Limnol.*

3   *Oceanogr.,* **12,** 537-539.

4   Meehl, G. A., and coauthors, 2007: The WCRP CMIP3 multimodel dataset - A new era in

5   climate change research. *Bull. Amer. Meteor. Soc.,* **88,** 1383-1394.

6   Moorthi, S., and M. J. Suarez, 1992: Relaxed Arakawa-Schubert: A parameterization of

7   moist convection for general circulation models. *Mon. Wea. Rev.,* **120,** 978-1002.

8   Morioka, Y., T. Tozuka, and T. Yamagata, 2010: Climate variability in the Southern Indian

9   Ocean as revealed by Self-Organizing Maps. *Climate Dyn.*, **35**, 1075-1088.

10   Morioka, Y., T. Tozuka, and T. Yamagata, 2011: On the growth and decay of the subtropical

11   dipole mode in the South Atlantic. *J. Climate*, in press.

12   Pelegri, J. L., A. Marrero-Diaz, and A. W. Ratsimandresy, 2006: Nutrient irrigation of the

13   North Atlantic. *Prog. Oceanogr.*, **70,** 366-406.

14   Philander, S. G. H., and R. C. Pacanowski, 1981: The oceanic response to cross-equatorial

15   winds (with application to costal upwelling in low latitudes). *Tellus,* **33**, 201-210.

16   Pradhan, Y., S. J. Lavender, N. J. Hardman-Mountford, and J. Aiken, 2006: Seasonal and

17   inter-annual variability of chlorophyll-a concentration in the Mauritanian upwelling:

18   observation of an anomalous event during 1998-1999. *Deep-Sea Res. II*, **53,** 1548-1559.

19   Qu, T., H. Mitsudera, and B. Qiu, 2001: A climatology of the Kuroshio/Oyashio system east

20   of Japan. *J. Phys. Oceanogr.,* **31,** 2575-2589.

1   Rayner, N. A., and Coauthors, 2003: Global analyses of sea surface temperature, sea ice,

2   and night marine air temperature since the late nineteenth century. *J. Geophys. Res.*, **108**,

3   doi:10.1029/2002JD002670.

4   Richter, I., and S. P. Xie, 2008: On the origin of equatorial Atlantic biases in coupled

5   general circulation models. *Climate Dyn.*, **31**, 587-598.

6   Richter, I., S. K. Behera, Y. Masumoto, B. Taguchi, N. Komori, and T. Yamagata, 2010: On

7   the triggering of Benguela Niños – remote equatorial vs. local influences. *Geophys. Res.*

8   *Lett.*, **37**, doi:10.1029/2010GL044461.

9   Richter, I., S. P. Xie, A. T. Wittenberg, and Y. Masumoto, 2011: Tropical Atlantic biases and

10   their relation to surface wind stress and terrestrial precipitation. *Climate Dyn.*, in press.

11   Rossow, W.B., L.C. Garder, P.J. Lu, and A.W. Walker, 1991: International Satellite Cloud

12   Climatology Project (ISCCP) Documentation of Cloud Data. WMO/TD-No. 266, World

13   Meteorological Organization, 76 pp. plus appendices. http://badc.nerc.ac.uk/view/-

14   badc.nerc.ac.uk__ATOM__dataent_isccp_d2

15   Rouault, M., P. Florenchie, N. Fauchereau, and C. J. C. Reason, 2003: South east tropical

16   Atlantic warm events and southern African rainfall. *Geophys. Res. Lett.*, **30,** doi:

17   10.1029/2002GL014840.

18   Russell, J. L., R. J. Stouffer, and K. W. Dixon, 2006: Intercomparison of the Southern

19   Ocean Circulations in IPCC Coupled Model Control Simulations. *J. Climate*, **19**,

20   4560–4575.

1   Servain, J., 1991: Simple climatic indices for the tropical Atlantic-ocean and some

2   applications. *J. Geophys. Res.,* **96,** 15137-15146.

3   Siedler, G., N. Zangenberg, and R. Onken, 1992: Seasonal changes in the tropical Atlantic

4   circulation: observation and simulation of the Guinea Dome. *J. Geophys. Res.,* **97,** 703-

5   715.

6   Signorini, S. R., R. G. Murtugudde, C. R. McClain, J. R. Christian, J. Picaut, and A. J.

7   Busalacchi, 1999: Biological and physical signatures in the tropical and subtropical

8   Atlantic. *J. Geophys. Res*., **104,** 18,367-18,382.

9   Simmons, A. J. J. K. Gibson, 2000: The ERA-40 Project Plan. In: The ERA-40 Project

10   Report Series, Nr. 1. http://www.ecmwf.int/research/era/Project/Plan/index.html.

11   Smith, T. M., R. W. Reynolds, T. C. Peterson, J. Lawrimore, 2008: Improvements to

12   NOAA's Historical Merged Land–Ocean Surface Temperature Analysis (1880–2006). *J.*

13   *Climate*, **21,** 2283-2296.

14   Stockdale, T. N., M. A. Balmaseda, and A. Vidard, 2006: Tropical Atlantic SST prediction

15   with coupled ocean-atmosphere GCMs. *J. Climate*, **19**, 6047-6061.

16   Stouffer R. J., and Coauthors, 2006: GFDL's CM2 global coupled climate models. Part IV:

17   Idealized climate response. *J. Climate,* **19,** 723–740.

18   Sutton R. T., and D. L. R. Hodson, 2005: Atlantic Ocean forcing of North American and

19   European summer climate. *Scinece*, **309**, 115-118.

20   Sutton R. T., and D. L. R. Hodson, 2007: Climate response to basin-scale warming and

1   cooling of the North Atlantic Ocean. *J. Climate*, **20**, 891-907.

2   Sweeney, C., A. Gnanadesikan, S. M. Griffies, M. J. Harrison, A. J. Rosati, and B. L.

3   Samuels, 2005: Impacts of shortwave penetration depth on large-scale ocean circulation

4   and heat transport. *J. Phys. Oceanogr.,* **35,** 1103-1119.

5   Tozuka, T., T. Miyasaka, A. Chakraborty, M. Mujumdar, S. K. Behera, Y. Masumoto, H.

6   Nakamura, and T. Yamagata, 2006: University of Tokyo Coupled General Circulation

7   Mode (UTCM1.0). *Ocean-atmosphere research report No. 7.*

8   Tozuka, T., T. Doi, T. Miyasaka, N. Keenlyside, and Toshio Yamagata, 2011: How to

9   simulate the equatorial Atlantic zonal SST gradient realistically in a coupled GCM. *J.

10   Geophys. Res.,* **116**, doi:10.1029/2010JC006717.

11   Vecchi, G. A., and B. J. Soden, 2007: Effect of remote sea surface temperature change on

12   tropical cyclone potential intensity. *Nature*, **450**, 1066-1070.

13   Vecchi, G. A., M. Zhao, G. Villarini, A. Rosati, I. Held, and R. Gudgel, 2011: Hybrid

14   statistical-dynamical predictions of seasonal Atlantic hurricane activity. *Mon. Wea. Rev.,*

15   **139**, 1070-1082.

16   Vimont, D. J., and J. P. Kossin, 2007: The Atlantic Meridional Mode and hurricane activity.

17   *Geophys. Res. Lett.*, doi:10.1029/2007GL029683.

18   Xie, P., and P. A. Arkin, 1997: Global precipitation: a 17-year monthly analysis based on

19   qauge observations, satellite estimates, and numerical model outputs. *Bull. Amer.

20   Meteor. Soc.*, **78**, 2539-2558.

1   Xie, S. P., 1999: A dynamic ocean-atmosphere model of the tropical Atlantic decadal

2   variability. *J. Climate*, **12,** 64-70.

3   Xie, S. P., and J. A. Carton, 2004: Tropical Atlantic variability: patterns, mechanisms, and

4   impacts. *Earth's Climate: The Ocean-Atmosphere Interaction: From Basin to Global*

5   *Scales, Geophys. Monogr., Vol. 147, Amer. Geophys. Union*, 121-142.

6   Yamagata, T., and S. Iizuka, 1995: Simulation of the tropical thermal domes in the Atlantic:

7   A seasonal cycle. *J. Phys. Oceanogr.*, **25,** 2129-2140.

8   Yu, L., X. Jin, and R. A. Weller, 2006: Role of net surface heat flux in seasonal variations of

9   sea surface temperature in the tropical Atlantic Ocean. *J. Climate*, **19,** 6153-6169.

10   Zebiak, S. E., 1993: Air-sea interaction in the equatorial Atlantic region. *J. Climate*, **6,**

11   1567-1586.

12   Zhang, R., and. T. L. Delworth, 2006: Impact of Atlantic multidecadal oscillations on

13   India/Sahel rainfall and Atlantic hurricanes. *Geophys. Res. Lett.*, **33**,

14   doi:10.1029/2006GL026267.

15   Zhang, R., T. L. Delworth, and I. M. Held, 2007: Can the Atlantic Ocean drive the observed

16   multidecadal variability in Northern Hemisphere mean temperature? *Geophys. Res.*

17   *Lett.*, **34**, doi:10.1029/2006GL028683.

18   Zhang, S., M. J. Harrison, A. Rosati, and A. Wittenberg, 2007: System Design and

19   Evaluation of Coupled Ensemble Data Assimilation for Global Oceanic Climate Studies.

20   *Mon. Wea. Rev.*, **135**, 3541–3564.

1   Zhang, S., and A. Rosati, 2010: An inflated ensemble filter for ocean data assimilation with

2   a biased coupled GCM. *Mon. Wea. Rev.*, **138**, 3905–3931.

Tables

Table 1: Summary for CM2.1 and CM2.5 biases in boreal spring. (a) The zonal wind stress along the Atlantic equator, averaged in 50°W-10°E, 2°S-2°N (N m^{-2}). Easterly wind is positive. (b) The meridional wind stress along the southeastern African coast, averaged in 5°-10°E, 10°S-0° (N m^{-2}). Southerly wind is positive. (c) The precipitation over northern South America, averaged in 75°-55°W, 10°S-10°N (mm day^{-1}). (d) The precipitation over the Congo basin, averaged in 10°W-40°E, 5°S-5°N (mm day^{-1}).

	Obs.	CM2.1	CM2.5
(a) Easterly wind stress along the equator (N m^{-2})	0.014 (NCEP/NCAR) 0.016 (ERA40)	0.0033	0.0068
(b) Southerly wind stress along the African coast (N m^{-2})	0.033 (NCEP/NCAR) 0.030 (ERA40)	0.0061	0.0093
(c) Northern South America Rainfall (mm day^{-1}).	7.0 (CMAP) 7.9 (GPCP)	5.1	6.1
(d) Congo Rainfall (mm day^{-1}).	5.1 (CMAP) 4.8 (GPCP)	5.0	5.2

1 **Table 2**: Summary for the interannual variations of the northern tropical Atlantic SST in

2 ERSSTv3, HadISST, CM2.1 and CM2.5. (a) The peak month when the interannual

3 variations of the northern tropical Atlantic SST show the maximum. (b) The standard

4 deviations of the interannual variations of the northern tropical Atlantic SST in the peak

5 month. (c) Warm years of the northern tropical Atlantic SST used for a composite analysis.

6 Also, the number of year per decade is shown. (d) Same as (c), but for cold years

	Observation	CM2.1	CM2.5
(a) Peak month	April (ERSSTv3) April (HadISST)	May	March
(b) Std. in peak month	0.54 (ERSSTv3) 0.56 (HadISST)	0.62	0.53
(c) Warm year	6 years (69, 70, 79, 80, 83, and 88) 1.4 year/decade	52 years 1.7 year/decade	48 years 1.7 year/decade
(d) Cold year	5 years (68, 74, 85, 86, 89) 1.2 year/decade	41 years 1.4 year/decade	41 years 1.5 year/decade

7

1 **Table 3**: The ocean dynamics contribution for the mixed-layer heat budget anomaly

2 averaged in the northern tropical Atlantic during July of the warm composite year (10^{-7} K s^{-}

3 ^{1}). Each term is calculated as in Appendix-1. Positive (negative) value denotes warming

4 (cooling) tendency. Boldface shows values beyond 99% significance levels.

	Total (10^{-7} K s^{-1})	$(W_{ent})' * \overline{\left(\dfrac{T_{mld}-T_d}{H_{mld}}\right)}$	$\overline{(W_{ent})} * \left(\dfrac{T_{mld}-T_d}{H_{MLD}}\right)'$	$(\vec{U}\cdot\nabla T_{mix})'$	Residual
Obs.	-0.12 (NCEP) +0.096 (ERA40) -0.018 (OAFlux-N) -0.010 (OAFlux-E)				
CM2.1	**+0.41**	**+0.32**	+0.14	-0.045	-0.005
CM2.5	**+0.30**	**+0.20**	+0.086	-0.045	+0.006

Figure captions

Fig. 1: (a) Annual mean SST from the ERSSTv3 data (°C). The contour interval is 1°C. (b) Annual mean rainfall from the CMAP data (mm day^{-1}). The contour interval is 1mm day^{-1}. The Sahel rainfall region (20°W-10°E, 10°-20°N) and the northern South America (75°-55°W, 10°S-10°N) are shown by boxes. (c) Same as (a), but for the HadISST data. (d) Same as (b), but for the GPCP data. (e) Same as (a), but for GFDL-CM2.1. (f) Same as (b), but for CM2.1. (g) Same as (a), but for CM2.5. (h) Same as (b), but for CM2.5.

Fig. 2: (a) Annual mean SST bias in CM2.1 from the ERSSTv3 data (°C). The contour interval is 1°C. (b) Annual mean rainfall bias in CM2.1 from the CMAP data (mm day^{-1}). The contour interval is 1mm day^{-1}. The Sahel rainfall region (20°W-10°E, 10°-20°N) and the northern South America (75°-55°W, 10°S-10°N) are shown by boxes. (c) Same as (a), but for CM2.5. (d) Same as (b), but for CM2.5.

Fig. 3: (a) Horizontal map of the standard deviation of the monthly averaged climatology of SST from the ERSSTv3 data (°C). The contour interval is 0.2°C. The Northern Tropical Atlantic region (NTA: 35°-18°W, 5°-20°N), the Atlantic Niño index (ATL3: 20°W-0°, 3°S-3°N), and the Angola-Benguela area (ABA: 0°-12°E, 25°-5°S) are shown in boxes. (b) Same as (a), but from the HadISST data. (c) Same as (a), but for GFDL-CM2.1. (d)

1 Same as (a), but for CM2.5.

2

3 **Fig. 4**: (a) Rate of change of SST averaged in the northern tropical Atlantic, 35°-18°W, 5°-

4 20°N (10^{-7}K s^{-1}). Rate of change of SST is determined by (b) surface enthalpy flux

5 contribution and (c) ocean dynamical contribution (Appendix-1). (d) Mixed-layer depth

6 averaged in the northern tropical Atlantic (m). (e) Annual cycle of net surface enthalpy

7 flux averaged in the northern tropical Atlantic (W m^{-2}). (f) Annual cycle of latent heat

8 flux (W m^{-2}). Negative value shows heat loss from ocean. (g) Same as (f), but for net

9 shortwave radiation (W m^{-2}). (h) Same as (f), but for total cloud amount (%).

10 Observational estimates are shown by dashed line.

11

12 **Fig. 5**: (a) Climatology of wind stress (N m^{-2}; vector) and Ekman upwelling (shaded; 10^{-6} m

13 s^{-1}) in July-September from the NCEP/NCAR reanalysis data. Upwelling is shown by

14 blue shading, while downwelling is shown by red shading. (b) Climatology of

15 stratification around mixed-layer depth, $\dfrac{T_{mix}-T_e}{H_{mix}}$, averaged in July-September from the

16 WOA05 data (10^{-2} K m^{-1}). The contour interval is 0.2×10^{-2}K m^{-1}. (c) Difference in

17 climatology of wind stress (N m^{-2}; vector) and Ekman upwelling (shaded; 10^{-6} m s^{-1}) in

18 July-September in the ERA40 reanalysis data minus the NCEP/NCAR reanalysis data.

19 (d) Same as (b), but for assimilation data of the CDAv3. (e) Same as (c), but for CM2.1

20 bias from the NCEP/NCAR reanalysis data. (f) Same as (b), but for CM2.1. (g) Same as

1   (e), but for CM2.5. (h) Same as (b), but for CM2.5.

2

3   **Fig. 6**: (a) Seasonal meridional migration of rainfall averaged in 50°-20°W from the CMAP

4   data (mm day^{-1}). The contour interval is 1 mm day^{-1}. (b) Seasonal meridional migration

5   of SST averaged in 50°-20°W from the ERSSTv3 (°C). The contour interval is 0.5°C.

6   (c) Seasonal meridional migration of Ekman upwelling averaged in 50°-20°W from the

7   NCEP/NCAR reanalysis data (10^{-6} m s^{-1}). The blue (red) shading denotes upwelling

8   (downwelling). The contour interval is 1×10^{-6}m s^{-1}. Green line shows location of ITCZ

9   which is defined as zero meridional wind stress averaged in 50°-20°W. (d) Same as (a),

10   but for the GPCP data. (e) Same as (b), but for the HadISST data. (f) Same as (c), but

11   for the ERA40 data. (g) Same as (a), but for GFDL-CM2.1. (h) Same as (b), but for

12   CM2.1. (i) Same as (c), but for CM2.1. (j) Same as (a), but for CM2.5. (k) Same as (b),

13   but for CM2.5. (l) Same as (c), but for CM2.5.

14

15   **Fig.7**: Same as Fig. 4, bur for ATL3 (20°-0°W, 3°S-3°N).

16

17   **Fig.8:** Same as Fig. 4, bur for ABA (0°-12°E, 25°-5°S).

18

19   **Fig. 9:** (a) Annual cycle of rainfall averaged in the Sahel region (20°W-10°E, 10°-20°N)

20   (mm day^{-1}). This index is also used in Lu and Delworth (2005). (b) Same as (a), but for

1   the northern South America region: 75°-55°W, 10°S-10°N.

2

3   **Fig. 10**: (a) Horizontal map of the standard deviation of the interannual SST anomaly

4   averaged in whole season from the ERSSTv3 data (°C). Contour interval is 0.2°C. The

5   northern tropical Atlantic region (NTA: 35°-18°W, 5°-20°N), the Atlantic Niño index

6   (ATL3: 20°W-0°, 3°S-3°N), and the Angola-Benguela area (ABA: 0°-20°E, 25°-5°S)

7   are shown in boxes. (b) Same as (a), but in August. (c) Same as (a), but for the

8   HadISST data. (d) Same as (b), but for the HadISST data. (e) Same as (a), but for

9   GFDL-CM2.1. (f) Same as (b), but for CM2.1.   (g) Same as (a), but for CM2.5. (h)
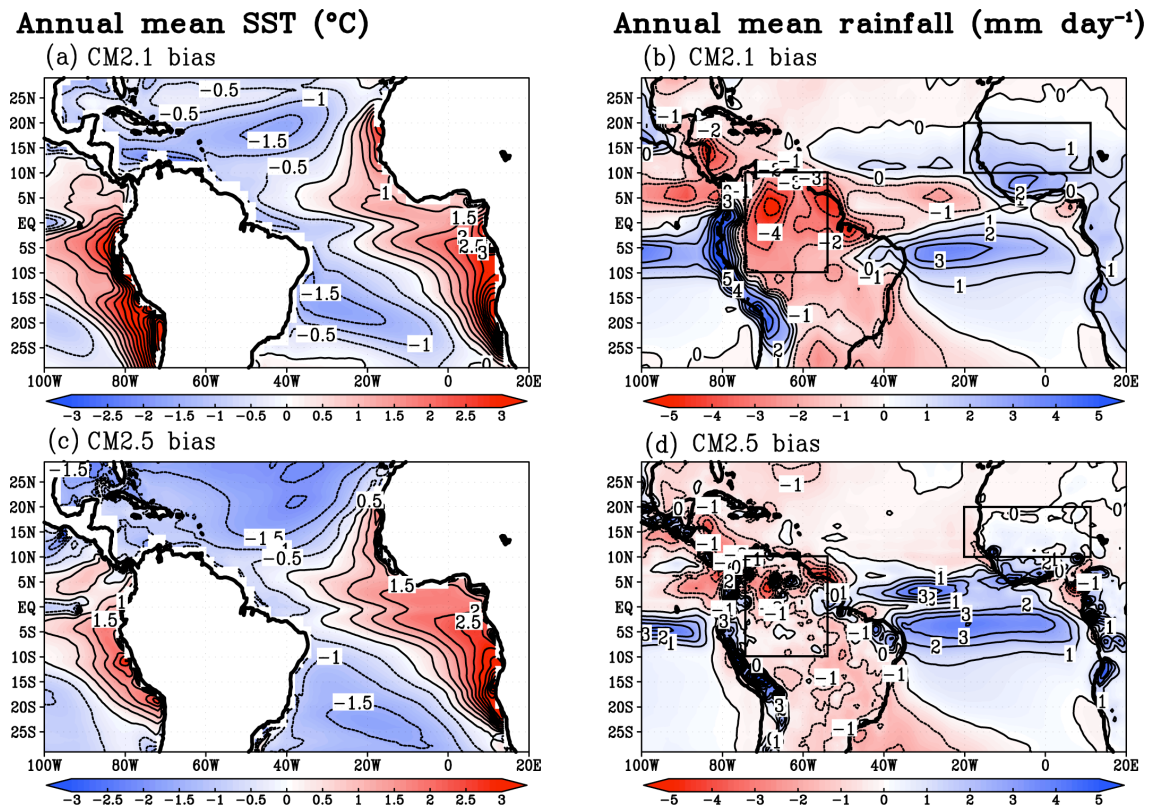
10   Same as (b), but for CM2.5.

11

12   **Fig. 11**: (a) Monthly standard deviation of the interannual variation of SST averaged in the

13   northern tropical Atlantic region (NTA: 35°-20°W, 5°-20°N) from ERSSTv3 (bar),

14   HadISST (grey line), GFDL-CM2.1 (red line), and CM2.5 (blue line) (°C). (b) Same as

15   (a), but for the Atlantic Niño index (ATL3: 20°W-0°, 3°S-3°N). (c) Same as (a), but for

16   the Angola-Benguela region (ABA: 0°-20°E, 25°-5°S).

17

18   **Fig.12**: Same as Fig. 4, but for composite anomalies in warm NTA SST years.

19

20   **Fig. 13**: (a) Composite anomalies for the net surface enthalpy flux from NCEP/NCAR

reanalysis data in February of warm NTA SST years (W m^{-2}). Positive values shows warming ocean. Contour interval is 5W m^{-2}. Color shading denotes anomalies above 90% significance level. (b) Same as (a), but for latent heat flux. (c) Same as (a), but for wind stress (N m^{-2}; vector). Red (blue) shading denotes weak (strong) anomalies above 90% significance. (d) Same as (a), but for ERA40 reanalysis data. (e) Same as (d), but for ERA40 reanalysis data. (f) Same as (c), but for ERA40 reanalysis data. (g) Same as (a), but for GFDL-CM2.1. Color shading denotes anomalies above 99% significance level. (h) Same as (g), but for latent heat flux. (i) Same as (c), but for CM2.1. Red (blue) shading denotes weak (strong) anomalies above 99% significance. (j) Same as (g), but for GFDL-CM2.5. (k) Same as (h), but for CM2.5. (l) Same as (i), but for CM2.5.

Fig.14: (a) Composite anomalies for Ekman upwelling in July of warm NTA SST years from NCEP/NCAR reanalysis data (shaded; 10^{-6}m s^{-1}). Red (blue) shading denotes downwelling (upwelling) anomalies. Contour shows climatology of stratification around mixed-layer depth, $\frac{T_{mix} - T_e}{H_{mix}}$, in July from WOA05 data (10^{-2}K m^{-1}). Contour interval is 1×10^{-2}K m^{-1}. (b) Same as (a), but for ERA40 reanalysis data and assimilation data of CDAv3. (c) Same as (a), but for GFDL-CM2.1. (d) Same as (a) but for GFDL-CM2.5.

1 **Fig.15**: (a) Same as Fig.9a, but for composite anomaly in warm NTA year. (b) Same as

2 Fig.9b, but for composite anomaly in warm NTA year.

3

4 **Fig.16:** Schematic diagram for (a) the realistic decay mechanism of the warm SST in the

5 northern tropical Atlantic linked with the Guinea Dome suggested by observational and

6 assimilated estimates. (b) The incorrect feedback linked with the Guinea Dome found in

7 CM2.1.
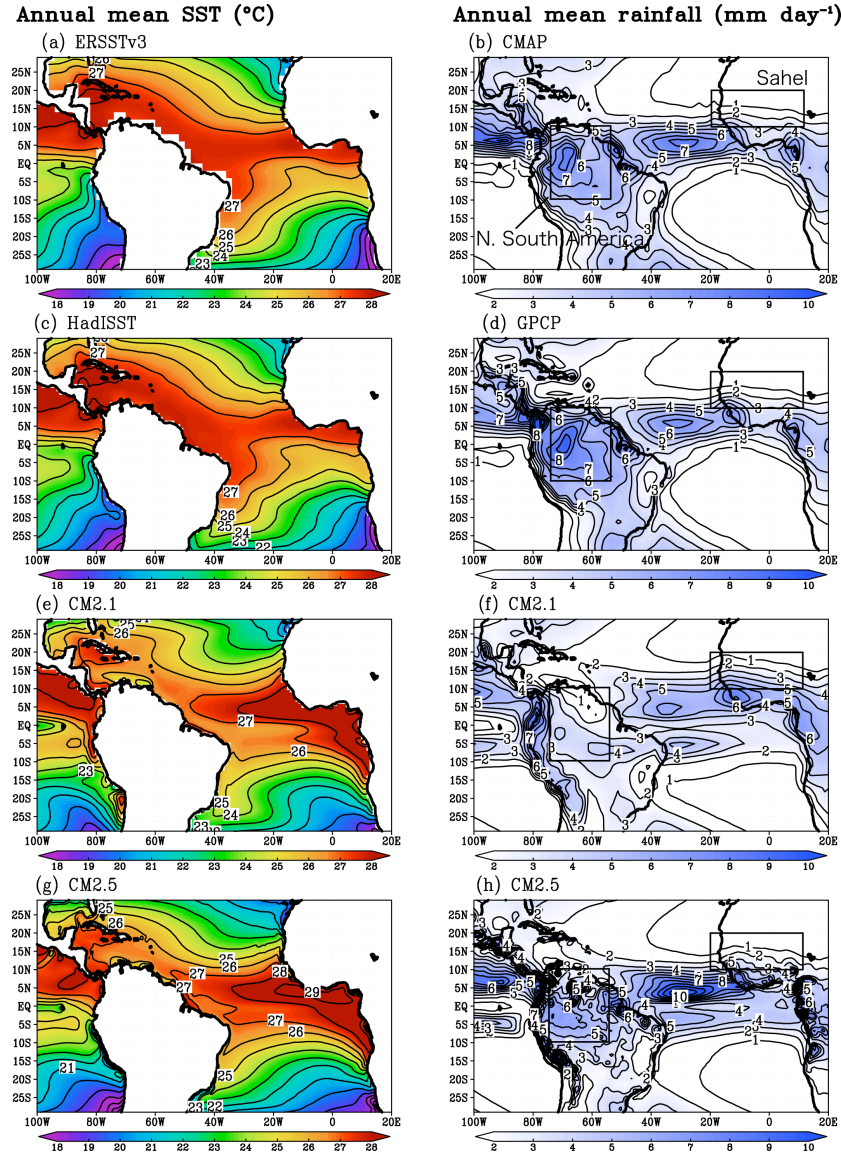
8

Figures

Fig.1

Fig. 1: (a) Annual mean SST from the ERSSTv3 data (°C). The contour interval is 1°C. (b) Annual mean rainfall from the CMAP data (mm day^{-1}). The contour interval is 1mm day^{-1}. The Sahel rainfall region (20°W-10°E, 10°-20°N) and the northern South America (75°-55°W, 10°S-10°N) are shown by boxes. (c) Same as (a), but for the HadISST data. (d) Same as (b), but for the GPCP data. (e) Same as (a), but for GFDL-CM2.1. (f) Same as (b), but for CM2.1. (g) Same as (a), but for CM2.5. (h) Same as (b), but for CM2.5.

Fig.2

Fig. 2: (a) Annual mean SST bias in CM2.1 from the ERSSTv3 data (°C). The contour interval is 1°C. (b) Annual mean rainfall bias in CM2.1 from the CMAP data (mm day⁻¹). The contour interval is 1mm day⁻¹. The Sahel rainfall region (20°W-10°E, 10°-20°N) and the northern South America (75°-55°W, 10°S-10°N) are shown by boxes. (c) Same as (a), but for CM2.5. (d) Same as (b), but for CM2.5.

Fig.3

Fig. 3: (a) Horizontal map of the standard deviation of the monthly averaged climatology of SST from the ERSSTv3 data (°C). The contour interval is 0.2°C. The Northern Tropical Atlantic region (NTA: 35°-18°W, 5°-20°N), the Atlantic Niño index (ATL3: 20°W-0°, 3°S-3°N), and the Angola-Benguela area (ABA: 0°-12°E, 25°-5°S) are shown in boxes. (b) Same as (a), but from the HadISST data. (c) Same as (a), but for GFDL-CM2.1. (d) Same as (a), but for CM2.5.

Fig.4

Seasonal variation in the northern tropical Atlantic (35°−18°E, 5°−20°N)
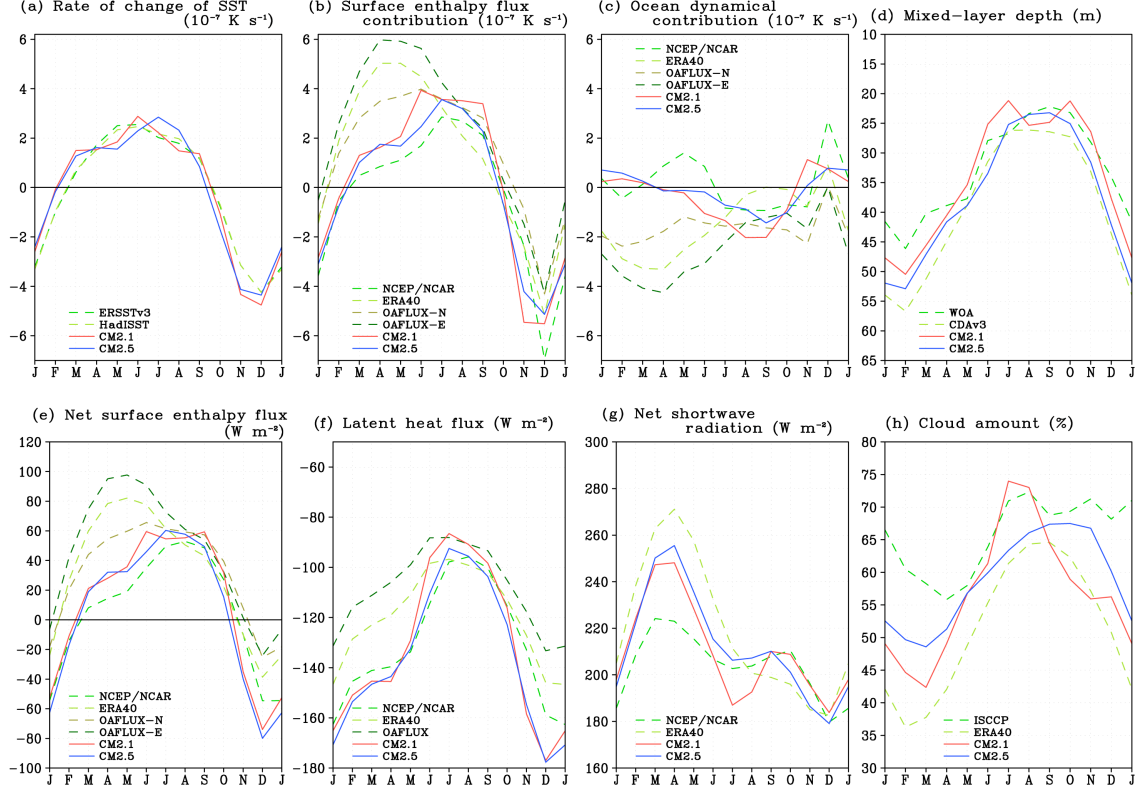
Fig. 4: (a) Rate of change of SST averaged in the northern tropical Atlantic, 35°-18°W, 5°-20°N (10^{-7}K s^{-1}). Rate of change of SST is determined by (b) surface enthalpy flux contribution and (c) ocean dynamical contribution (Appendix-1). (d) Mixed-layer depth averaged in the northern tropical Atlantic (m). (e) Annual cycle of net surface enthalpy flux averaged in the northern tropical Atlantic (W m^{-2}). (f) Annual cycle of latent heat flux (W m^{-2}). Negative value shows heat loss from ocean. (g) Same as (f), but for net shortwave radiation (W m^{-2}). (h) Same as (f), but for total cloud amount (%). Observational estimates are shown by dashed line.

Fig.5
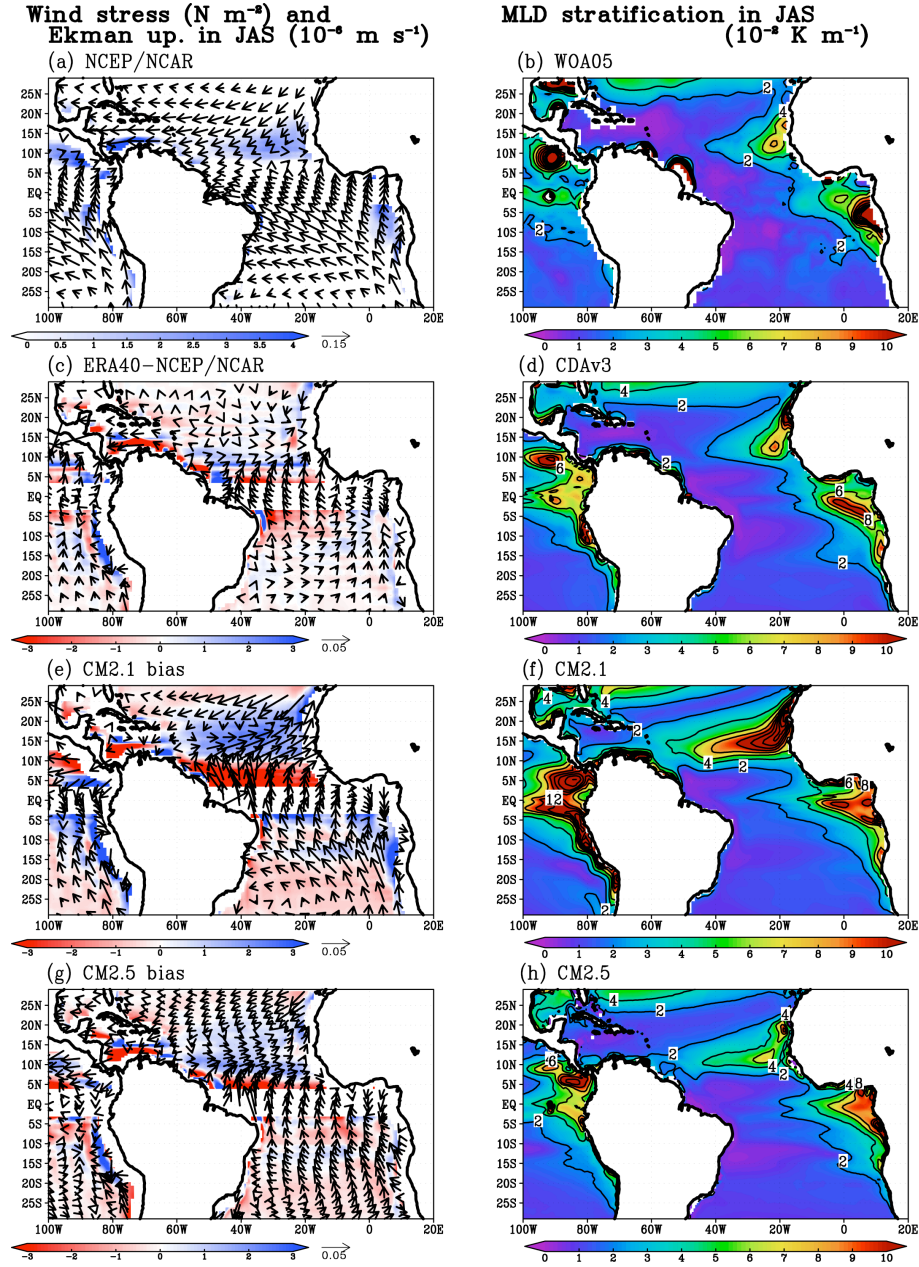
Fig. 5: (a) Climatology of wind stress (N m^{-2}; vector) and Ekman upwelling (shaded; 10^{-6} m s^{-1}) in July-September from the NCEP/NCAR reanalysis data. Upwelling is shown by blue shading, while downwelling is shown by red shading. (b) Climatology of stratification around mixed-layer depth, $\dfrac{T_{mix} - T_e}{H_{mix}}$, averaged in July-September from the

WOA05 data (10^{-2} K m^{-1}). The contour interval is 0.2×10^{-2}K m^{-1}. (c) Difference in climatology of wind stress (N m^{-2}; vector) and Ekman upwelling (shaded; 10^{-6} m s^{-1}) in July-September in the ERA40 reanalysis data minus the NCEP/NCAR reanalysis data. (d) Same as (b), but for assimilation data of the CDAv3. (e) Same as (c), but for CM2.1 bias from the NCEP/NCAR reanalysis data. (f) Same as (b), but for CM2.1. (g) Same as (e), but for CM2.5. (h) Same as (b), but for CM2.5.

Fig.6
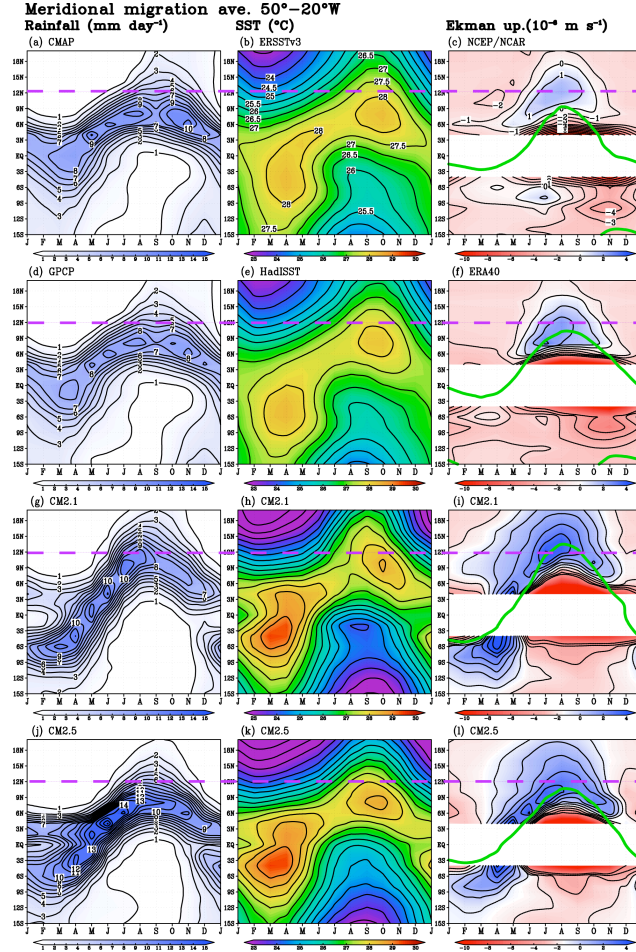
Fig. 6: (a) Seasonal meridional migration of rainfall averaged in 50°-20°W from the CMAP data (mm day^{-1}). The contour interval is 1 mm day^{-1}. (b) Seasonal meridional migration of SST averaged in 50°-20°W from the ERSSTv3 (°C). The contour interval is 0.5°C. (c) Seasonal meridional migration of Ekman upwelling averaged in 50°-20°W from the NCEP/NCAR reanalysis data (10^{-6} m s^{-1}). The blue (red) shading denotes upwelling (downwelling). The contour interval is 1×10^{-6} m s^{-1}. Green line shows location of ITCZ which is defined as zero meridional wind stress averaged in 50°-20°W. (d) Same as (a), but for the GPCP data. (e) Same as (b), but for the HadISST data. (f) Same as (c), but for the ERA40 data. (g) Same as (a), but for GFDL-CM2.1. (h) Same as (b), but for CM2.1. (i) Same as (c), but for CM2.1. (j) Same as (a), but for CM2.5. (k) Same as (b), but for CM2.5. (l) Same as (c), but for CM2.5.

Fig. 7

Seasonal variation in the equatorial Atlantic (20°−0°W, 3°S−3°N)
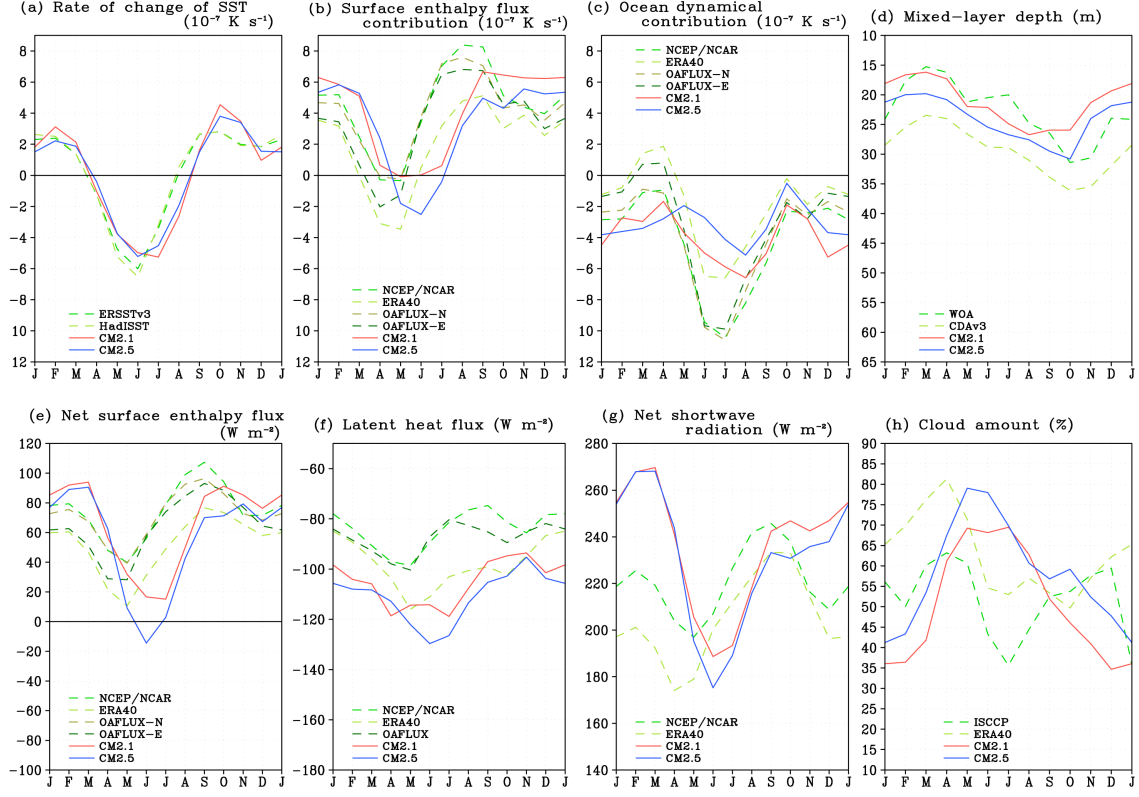
Fig.7: Same as Fig. 4, bur for ATL3 (20°-0°W, 3°S-3°N).

Fig. 8

Seasonal variation in the Angola−Benguela area (0°−12°E, 25°−5°S)
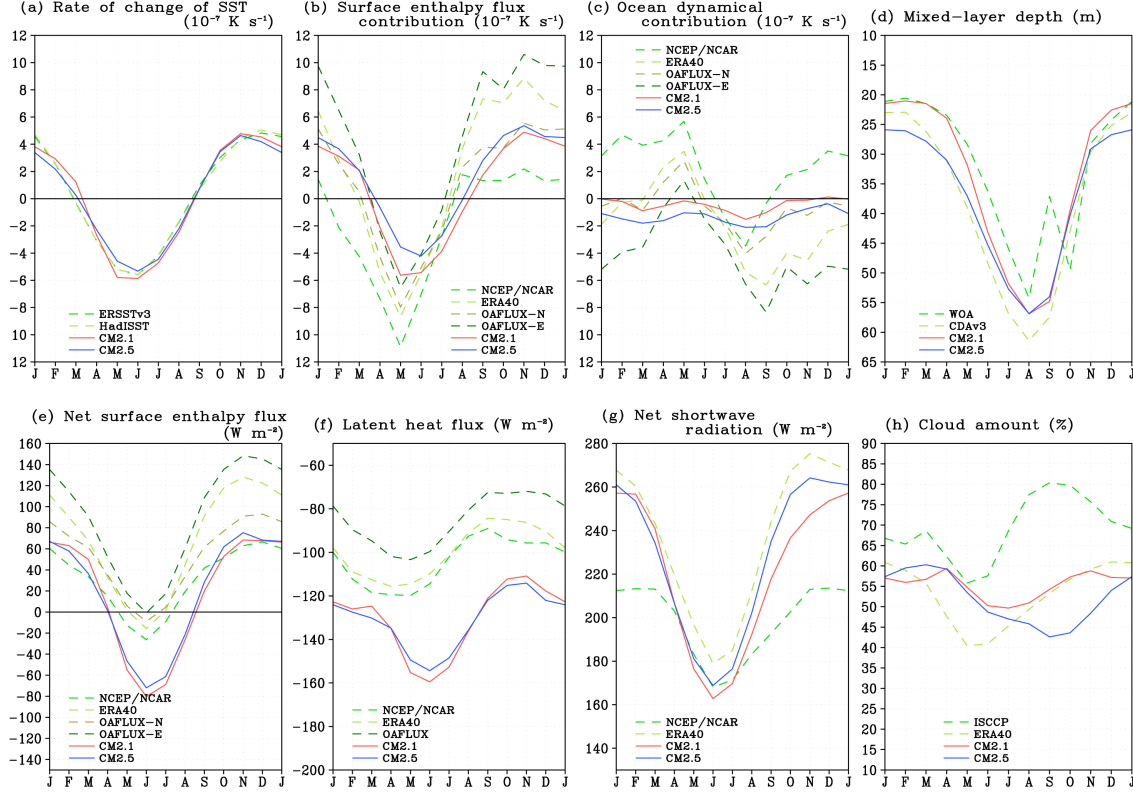
Fig.8: Same as Fig. 4, bur for ABA (0°-12°E, 25°-5°S).

Fig.9

Rainfall (mm day⁻¹)

(a) Sahel rainfall index (20°W−10°E,10°−20°N)

(b) N.South America rainfall index
(75°−55°W,10°S−10°N)
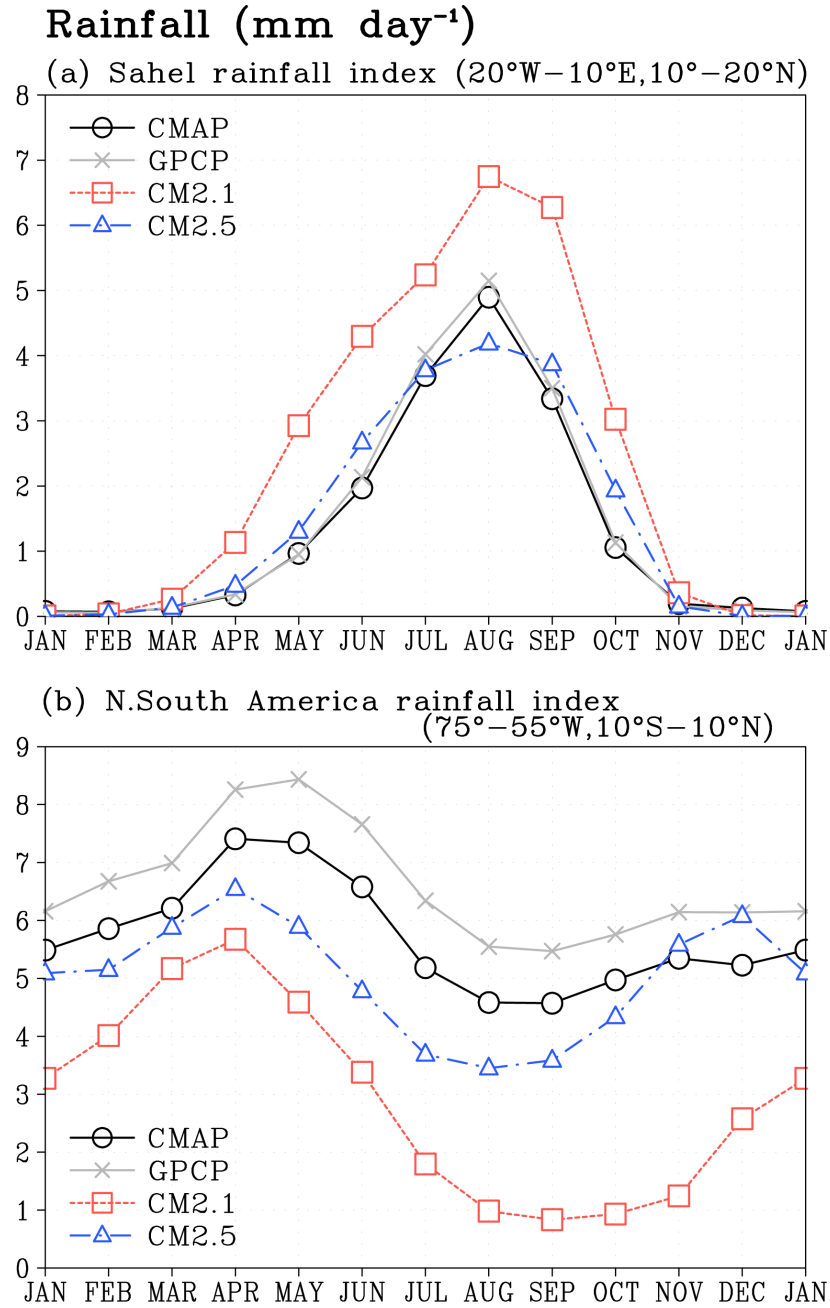
Fig. 9: (a) Annual cycle of rainfall averaged in the Sahel region (20°W-10°E, 10°-20°N) (mm day⁻¹). This index is also used in Lu and Delworth (2005). (b) Same as (a), but for the northern South America region: 75°-55°W, 10°S-10°N.

Fig.10
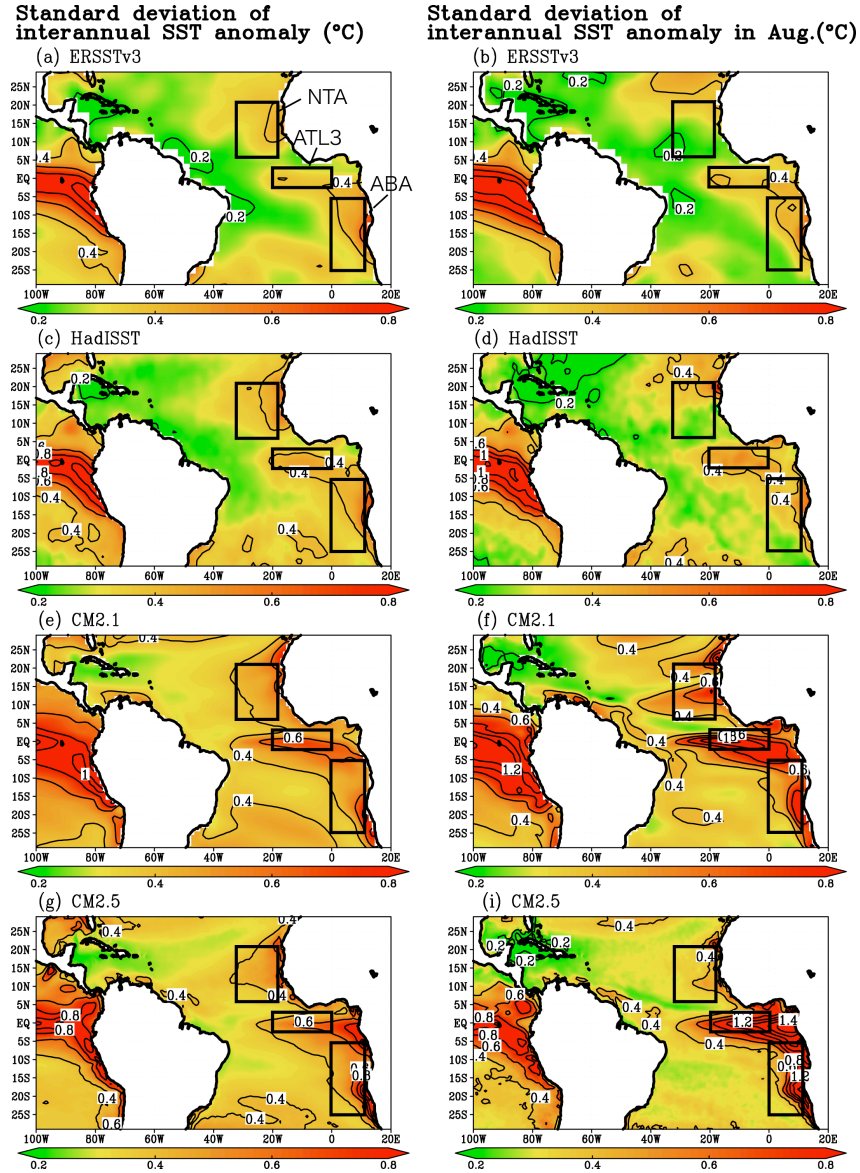
Fig. 10: (a) Horizontal map of the standard deviation of the interannual SST anomaly averaged in whole season from the ERSSTv3 data (°C). Contour interval is 0.2°C. The northern tropical Atlantic region (NTA: 35°-18°W, 5°-20°N), the Atlantic Niño index (ATL3: 20°W-0°, 3°S-3°N), and the Angola-Benguela area (ABA: 0°-20°E, 25°-5°S) are shown in boxes. (b) Same as (a), but in August. (c) Same as (a), but for the HadISST data. (d) Same as (b), but for the HadISST data. (e) Same as (a), but for GFDL-CM2.1. (f) Same as (b), but for CM2.1. (g) Same as (a), but for CM2.5. (h) Same as (b), but for

CM2.5.

Fig.11

**Standard deviation
of interannual SST variation (°C)**
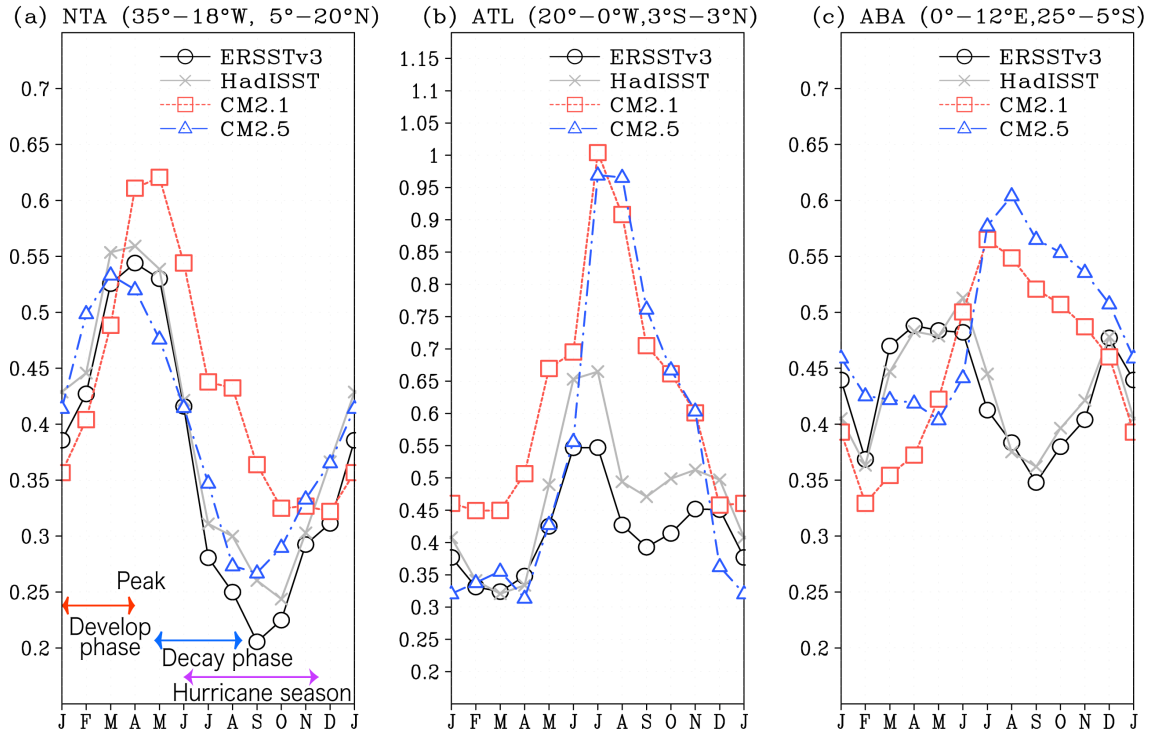
Fig. 11: (a) Monthly standard deviation of the interannual variation of SST averaged in the northern tropical Atlantic region (NTA: 35°-20°W, 5°-20°N) from ERSSTv3 (bar), HadISST (grey line), GFDL-CM2.1 (red line), and CM2.5 (blue line) (°C). (b) Same as (a), but for the Atlantic Niño index (ATL3: 20°W-0°, 3°S-3°N). (c) Same as (a), but for the Angola-Benguela region (ABA: 0°-20°E, 25°-5°S).

Fig.12

Warm year composite in the northern tropical Atlantic (35°−18°E, 5°−20°N)

Fig.12: Same as Fig. 4, but for composite anomalies in warm NTA SST years.

Fig.13

Feb. in warm year composite

Fig. 13: (a) Composite anomalies for the net surface enthalpy flux from NCEP/NCAR reanalysis data in February of warm NTA SST years (W m^{-2}). Positive values shows warming ocean. Contour interval is 5W m^{-2}. Color shading denotes anomalies above 90% significance level. (b) Same as (a), but for latent heat flux. (c) Same as (a), but for wind stress (N m^{-2}; vector). Red (blue) shading denotes weak (strong) anomalies above 90% significance. (d) Same as (a), but for ERA40 reanalysis data. (e) Same as (d), but for ERA40 reanalysis data. (f) Same as (c), but for ERA40 reanalysis data. (g) Same as (a), but for GFDL-CM2.1. Color shading denotes anomalies above 99% significance level. (h) Same as (g), but for latent heat flux. (i) Same as (c), but for CM2.1. Red (blue) shading denotes weak (strong) anomalies above 99% significance. (j) Same as (g), but for GFDL-CM2.5. (k) Same as (h), but for CM2.5. (l) Same as (i), but for CM2.5.
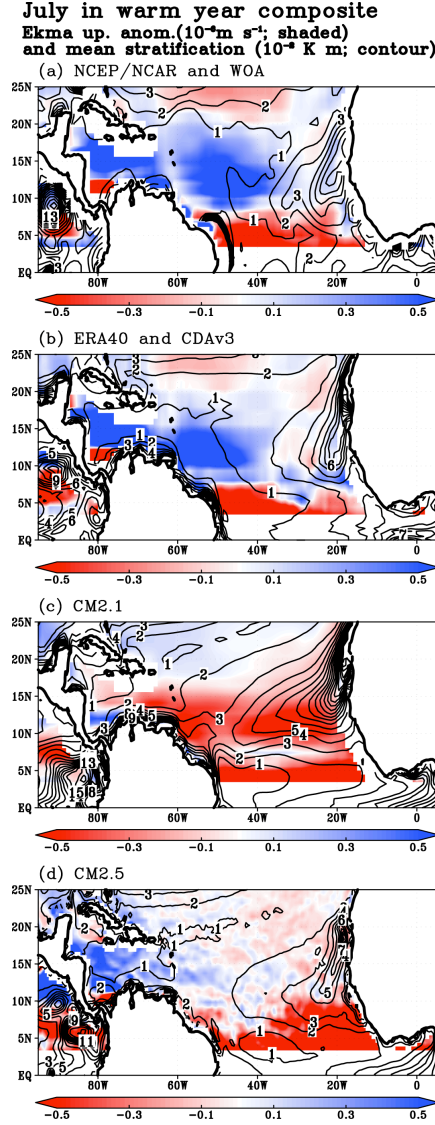
Fig.14

Fig.14: (a) Composite anomalies for Ekman upwelling in July of warm NTA SST years from NCEP/NCAR reanalysis data (shaded; 10^{-6}m s^{-1}). Red (blue) shading denotes downwelling (upwelling) anomalies. Contour shows climatology of stratification around mixed-layer depth, $\frac{T_{mix} - T_e}{H_{mix}}$, in July from WOA05 data (10^{-2}K m^{-1}). Contour interval is 1 $\times 10^{-2}$K m^{-1}. (b) Same as (a), but for ERA40 reanalysis data and assimilation data of CDAv3. (c) Same as (a), but for GFDL-CM2.1. (d) Same as (a) but for GFDL-CM2.5.
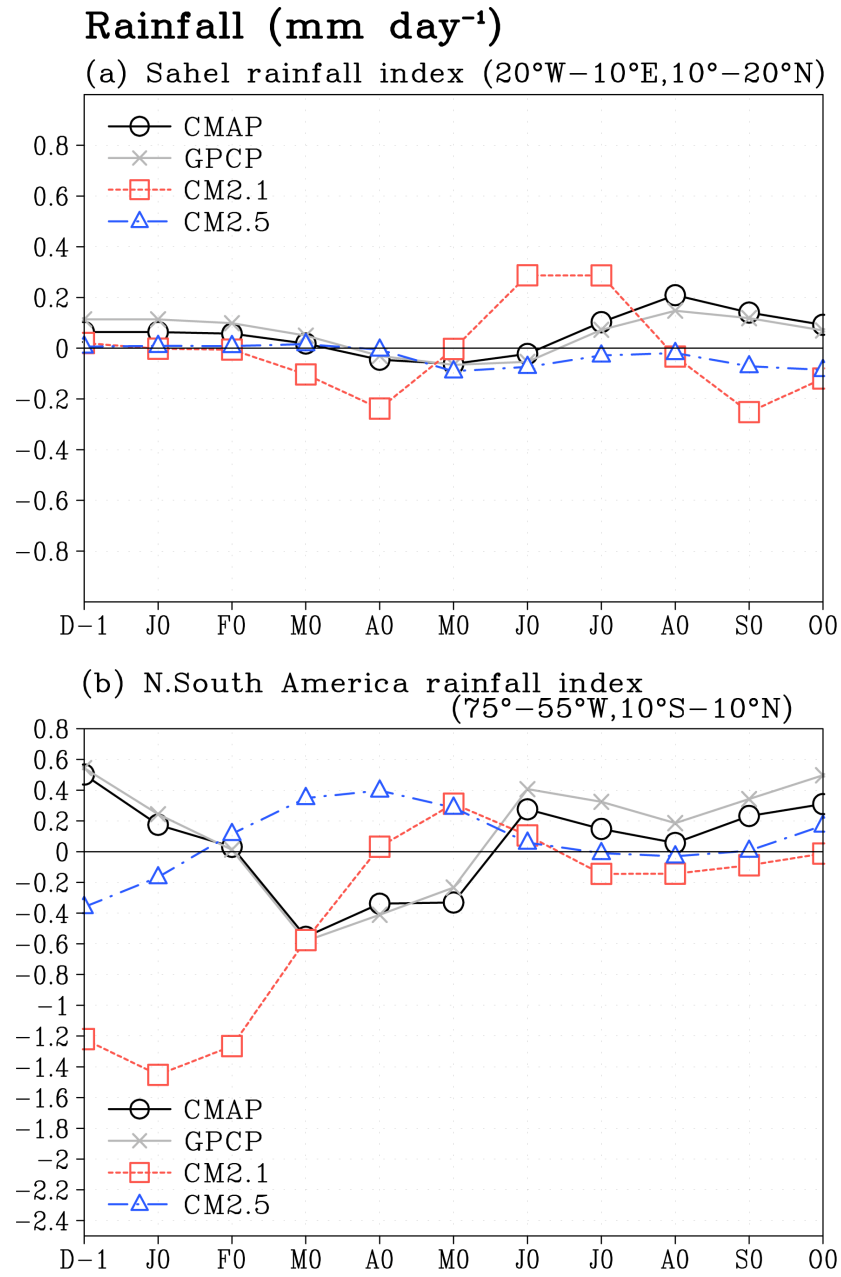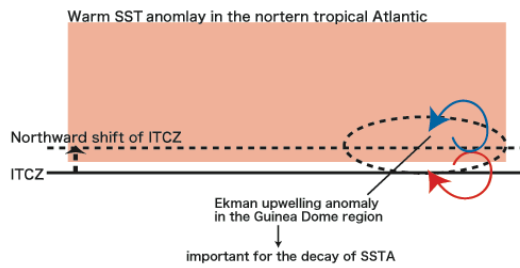
Fig. 15

Rainfall (mm day⁻¹)

(a) Sahel rainfall index (20°W−10°E,10°−20°N)

(b) N.South America rainfall index
(75°−55°W,10°S−10°N)

Fig.15: (a) Same as Fig.9a, but for composite anomaly in warm NTA year. (b) Same as Fig.9b, but for composite anomaly in warm NTA year.
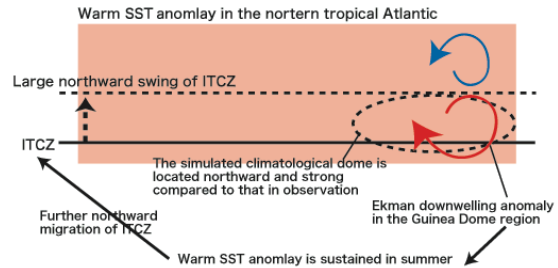
Fig. 16

Fig.16: Schematic diagram for (a) the realistic decay mechanism of the warm SST in the northern tropical Atlantic linked with the Guinea Dome suggested by observational and assimilated estimates. (b) The incorrect feedback linked with the Guinea Dome found in CM2.1.